Photonuclear processes in the treatment room and patient during radiation therapy with 50 MV photons.

Irena Gudowska
Department of Medical Radiation Physics
Karolinska Institute and Stockholm University
P.O. Box. 260, S - 171 76, Stockholm
Sweden

Slutrapport för projekt SSI P 858.94.
Titel: Beräkningar av energideponering i tumör och normalvävnad från fotonukleära reaktioner samt studier av neutrontransport i behandlingsrum i energiintervallet 10 - 50 MV.

Photonuclear processes in the treatment room and patient during radiation therapy with 50 MV photons.

Irena Gudowska
Department of Medical Radiation Physics
Karolinska Institute and Stockholm University

Summary.

During radiation therapy with high energy bremsstrahlung beams, above 10 MV, photonuclear reactions in the accelerator head and within the treated volume of the patient are a source of small but significant dose to the patient. The photoneutrons from the primary source in the accelerator head, generated mainly through (γ,xn) reactions, are transported and scattered inside the entire structure of the machine and the treatment room. In consequence the whole body of the patient is affected by neutrons coming directly from the treatment unit and neutrons scattered from the walls. In addition to these neutrons, photonuclear reactions in the body are a source of photonuclear particles (neutrons, protons, alphas) which deposit their energy directly to the tissue. These latter photonuclear reactions deliver a small absorbed dose to the patient which may also influence the relative biological effectiveness (RBE) during radiotherapy particularly with very high energy photons.

The objectives of this project were to determine the level of photoneutron radiation around the MM50 Racetrack microtron at Karolinska Hospital, Stockholm operating in different modes and to evaluate the photonuclear absorbed dose to the treated volume of the patient during radiation therapy with a 50 MV photon beam.

Photoneutron radiation in the treatment room of the MM50 Racetrack microtron has been studied both using the measurement technique with the ^{235}U fission chamber and by computer simulation.

Fast and thermal neutron fluence measurements have been performed for the different positions in the patient plane at 1 m SID (source-isocentre-distance) for the radiation field 10 x 10 cm^2 and the 50 MV photon beam operating in the scanned and stationary modes. The measurements were performed for two bremsstrahlung targets 9 mm Be + 6 mm W (9Be6W) and 5 mm W + 6.5 mm Cu (5.5W6.5W). All results of neutron fluence have been normalised to unit photon dose at dose maximum in the tissue.

The level of fast neutron fluence inside the treatment room varies from 2.0 at the isocentre to 0.1 times 10^7 neutrons cm^{-2} Gy^{-1} near the first shielding door in front of the maze, during operation with 50 MV photons in scanned mode and 9Be6W

target. In the maze, behind the first door, the measured neutron fluence is about 0.002×10^7 cm^{-2} Gy^{-1}, whereas outside the maze and behind the second shielding door about half of this value. The measured thermal neutron fluence inside the central part of the treatment room is almost independent of the distance from the isocenter and about ten times lower than the fast neutron fluence. The same level of neutron radiation is produced independent on target design.

The neutron fluence at the isocenter for the 50 MV photon beam and the 9Be6W target is about 4.5 times larger for the scanned mode than for the stationary mode. In the scanned mode a larger volume of shielding materials is penetrated by high energy photons and for a given photon dose at isocenter many more photons are emitted from the target when compared to the stationary mode. In consequence the higher photoneutron production is observed for the scanned mode.

The fast neutron fluences at the isocenter and at the distance 30 cm from the isocenter have also been determined for a wide range of the operating electron energies from 10 up to 50 MeV for the 9Be6W target and the scanned mode. These results show the increasing photoneutron production with the acceleration energy up to 30 MV. Between 30 and 50 MV almost constant neutron yield is observed in agreement with the other observations.

In order to estimate the photoneutron radiation risk to healthy tissues in the patient the neutron absorbed dose was calculated using the fluence-to-absorbed dose conversion factors from NCRP Report 79. For radiation therapy with 50 MV photons it was assumed that neutron spectrum in the patient plane has a mean energy of 1 MeV. The photoneutron absorbed dose to patient due to accelerator produced neutrons varies from about 0.044 to 0.013% of the photon dose at dose maximum in the distance range from 0 to 1 m from the isocenter for the scanned beam of 50 MV photons and the 9Be6W target.

For radiation safety aspects, both for the patient and the hospital personnel it is important to distinguish the principal sources of the photonuclear products and better understand the neutron transport inside the treatment room. For these purposes a computer simulation of neutron sources, neutron transport and neutron fluence inside the treatment room of a MM50 racetrack microtron has been performed using Monte Carlo codes and analytical calculations. The ITS 3.0 code was used to evaluate the bremsstrahlung spectrum from a 9Be6W target and to follow photon transport in the treatment head. The photoneutron sources in the treatment head were calculated analytically and neutron transport inside the treatment room and calculation of the fast neutron fluence were simulated using MCNP4A. For the scanned beam mode several simplifications, mainly concerning the geometry setup for the particle transport in the treatment head, were necessary

to apply due to bugs in the ITS 3.0 code for the oblique beam geometry. Because of this the bremsstrahlung spectrum was calculated for a pencil beam, impinging perpendicularly on the target and corrected later for the oblique beam geometry. In addition some simplified description of the geometry were needed since both codes ITS 3.0 and MCNP4A use different approach to describe the geometry setup for the problem. In consequence, this approach resulted in the very approximative determination of the photoneutron sources in the cells of the treatment head. The calculated fast neutron fluences in the patient plane are in the large discrepancy from the measured data by factor from 1.5 to 3.5 depending on the distance from the isocenter.

One of the goals in these studies was to determine the photonuclear dose to the tissue during radiation therapy with 50 MV photons and to calculate which photonuclear interactions with the tissue constituents are most significant. The observed RBE values ranging from 1.1 -1.2 for high energy bremsstrahlung beams (50 MV) by microdosimetric and radiobiological measurements using V79 and jejunal crypt cells suggests that photonuclear processes may have a significant role for the increased cell lethality.

The photonuclear dose due to photonuclear reactions (γ,xn), (γ,xp), (γ,np), (γ,xα) in the treated volume was evaluated for an average soft tissue in an adult male with the elemental composition (fraction by weight): 0.105 H, 0.256 C, 0.027 N, 0.602 O, 0.001 Na, 0.002 P, 0.003 S, 0.002 Cl, 0.002 K. Calculation of the bremsstrahlung production in the 9Be6W target for the scanned beam and photon transport was evaluated for a simplified geometry target - air - tissue equivalent phantom using the Monte Carlo code ITS 3.0. The photonuclear production of neutrons, protons, ^{4}He, ^{3}He and deuterons in the treated volume have been calculated using the photon energy spectrum in the tissue and the photonuclear cross section for the tissue constituents. The photoneutron transport and energy deposition to the tissue have been evaluated using the Monte Carlo code MCNP4A, whereas the photonuclear absorbed dose to the soft tissue due to other heavy photoparticles was calculated analytically assuming the charge particle equilibrium. The total photonuclear absorbed dose in tissue consists of the contributions due to photonuclear particles produced in tissue and due to photoneutrons produced in the accelerator and transported to the tissue. The calculated photonuclear absorbed doses in tissue at the depth 5.5 cm on the central axis due to neutrons, protons, ^{4}He and ^{3}He particles are about 0.015, 0.09, 0.005 and 0.00012 % of the maximum photon dose, respectively. The contribution due to accelerator produced neutrons is about 0.02 % of the photon maximum dose. The total photonuclear absorbed dose to patient at this depth is about 0.13% of the maximum photon dose.

In this evaluation the simplified geometry of the treatment head for the particle transport together with the calculation for a pencil beam impinging perpendicularly on the target instead of oblique beam geometry influence on the accuracy of the results.
Since the evaluations of the photoneutron fluences inside the treatment room and the photonuclear absorbed dose to tissue using this approach seems to be too approximative it would be useful to improve this calculation method by using the more powerful Monte Carlo codes like MCNP4B or FLUKA 93/94.

The estimated neutron equivalent dose due to accelerator produced neutrons by photon beams from MM50 Racetrack microtron delivered to the tissues inside and outside the treatment volume do not exceed the recommended values . However there is a potential risk that the sensitive tissues (lens of the eye or gonads), outside the treatment volume, can receive a dose of about 300 - 500 mSv per photon treatment course of 60 Gy_{γ} with a slightly increase for secondary malignancies.

Contents.

1. Introduction.

Medical electron accelerators operating above the energy threshold for photonuclear reactions typically 8 - 13 MeV in high Z and 18 - 23 MeV in low to medium Z materials are generating neutrons through (γ,xn) and (e,e'n) reactions. These reactions take place in the bremsstrahlung target, flattening filter, collimators and shielding materials inside the treatment head and in the patient [1]. The cross section for the production of neutrons by electronuclear interactions is about two orders of magnitude ($1/\alpha \approx 1/137$) lower than the corresponding photoneutron cross section, so the direct process (e,e'n) can generally be neglected, except possibly inside the bremsstrahlung target. The cross section for photoneutron production has generally a maximum related to giant resonance at an energy between 10 and 17 MeV for medium and high atomic number (Z) and between 20 and 26 MeV for low to medium Z ($6 \leq Z \leq 40$) materials. The primary photoneutron spectrum for high atomic number materials is qualitatively similar to a fission-neutron spectrum, like from ^{252}Cf source, but with a slightly higher mean energy of around 2.0 MeV [2]. The photoneutrons from the primary source in the accelerator head are diffusing through the accelerator head shield (W, Fe, Pb) and scattered on other structure of the treatment machine and the treatment room. In consequence the escaping filtered neutron spectrum is softened somewhat and the mean energy of the leakage photoneutron spectrum is reduced to about 0.5 - 1.0 MeV somewhat depending on the bremsstrahlung target and filter design [1, 3, 4].

During radiation therapy with high energy bremsstrahlung beams, above some 10 MV, the whole body of the patient is exposed to direct neutrons coming from the treatment unit and scattered neutrons from the walls. In addition to these neutrons, photonuclear reactions in the body are a source of photonuclearparticles (neutrons, protons, alphas) which deposit their energy directly to the tissue. These latter photonuclear reactions deliver a small absorbed dose to the patient which may also influence the relative biological effectiveness (RBE) during radiotherapy particularly with very high energy photons. The observed RBE values ranging from 1.1 -1.2 for high energy bremsstrahlung beams (50 MV) by microdosimetric [5] and radiobiological measurements using V79 and jejunal crypt cells [6] suggests that photonuclear processes may have a significant role for the increased cell lethality.
To improve the radiation safety of the patient and the hospital personnel, it is important to distinguish the principal sources of the photonuclear products and better understand the neutron transport inside the treatment room. The neutron contamination of high energy photon beams contributes to the total radiation dose delivered to the patient both inside and outside the treated volume. It is important to accurately determine the absorbed dose also in the zone surrounding the target

volume since high LET photonuclear particles reaching the patient body are associated with an increased risk of inducing cancer in healthy tissues.
Thermal neutron capture in the different materials of the treatment room or in the maze is also a significant source of gamma rays for the personnel [1]. A gamma ray level that is higher than the natural background is present in the treatment room at least 10 to 20 minutes after the photon beam is shut off, especially near the treatment head and walls directly irradiated by the photon beam.
Several investigations of the problems associated with neutron production in electron accelerators have been made during the last decades [7-23]. There is a renewed interest during the last few years, due to the increased use of high energy machines, to ensure that the effect on the personnel is negligible and the effects on the patient fully understood.

2. Neutron radiation measurements around the MM50 racetrack microtron, Karolinska Hospital , Stockholm.

2.1 The treatment unit.

The 50 MV racetrack microtron installed at the Karolinska Hospital (KS) provides electron and photon beams with maximum energies in the range 2 - 52 MeV initially in steps of 5.2 MeV. The accelerator is equipped with a beam scanning system instead of conventional flattening filters [24]. Large homogenous or intensity modulated fields are produced using different scanning matrices. The absence of flattening filters reduces the variation of the mean energy across the beam often seen in conventional accelerators with flattening filter and reduces the neutron production in the treatment head. The final beam shaping is achieved by a double focusing multileaf collimator with tungsten leaves together with a pair of block collimators of lead located closer to the target. Different composite targets for bremsstrahlung production have been used during the first period of operation: a standard W - Cu, a narrow high intensity beam Be - W, both fully stopping the electron beam, and a thin Be giving an extremely narrow photon beam requiring purging magnet for the transmitted high energy electrons.
Fig. 1 presents schematically the layout of the treatment head and gantry of the MM50 racetrack microtron.

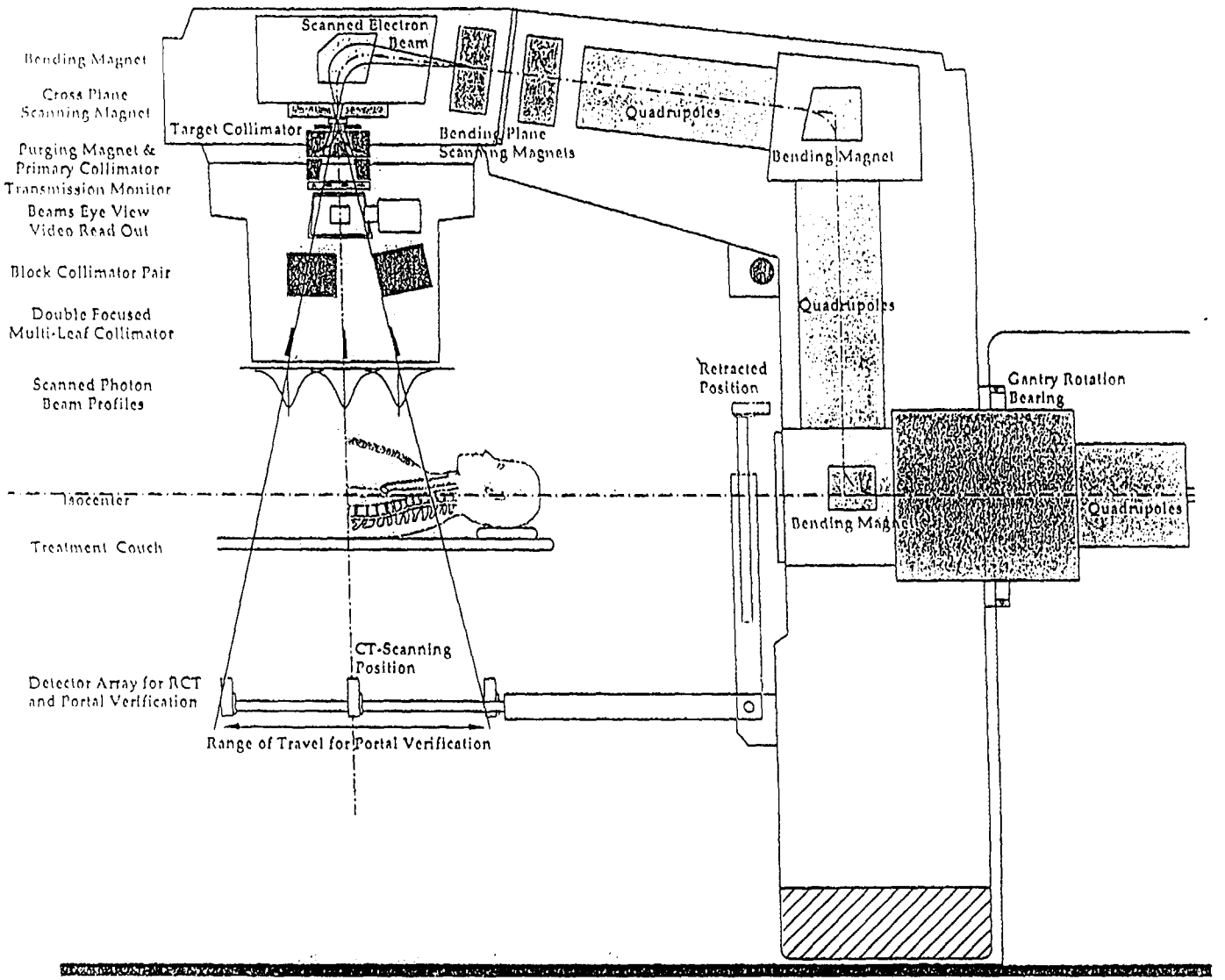

Fig. 1. Schematic drawing of the MM50 racetrack microtron in the bending plane of the treatment head.

2.2 Measurement method.

Measurements of the neutron contamination in the photon beam are difficult, since intense, pulsed, high energy, electromagnetic radiation seriously limits the types of neutron detectors possible due to disturbances like 'pile-up' effects and significant photoneutron production in the detector itself [7, 25]. For high energy X-ray beams the ratio of neutron to photon dose rate inside the primary beam is about 10^{-3}. Measurements outside the photon beam are easier to perform but still a high neutron sensitivity is required and an ability to work in pulsed radiation fields. In these measurements a neutron absorbed dose to tissue of 0.01 % of the photon absorbed dose at dose maximum has to be detected. The corresponding photon leakage at the measuring point outside the beam is about 0.1% of the maximum photon dose.

For these reasons, a passive detector like foil activation is the most reliable and common technique used in the clinical accelerator environments [4, 9, 13, 26, 27]. With a special shielding technique to remove or decrease the intense photon and lepton component, some active neutron monitors like small fission chambers are possible to use both inside and outside the primary photon beam [9, 11]. In such cases the applied photon and lepton shield is of a small mass and careful evaluation of photoneutron production in the detector shield has to be done.

The previous investigations [9] have shown that the results by the ^{235}U fission chamber method and the foil activation with In differ by less than 15% for 10x10 cm^2 field and less than 9% in the case of closed collimators. Since the use of the small detector in 'on - line' measurement is of great importance and very practical in clinical applications a ^{235}U fission chamber has been used in the present work for the neutron measurements inside the treatment room and in the maze.
For the measurements outside the treatment room, in the therapy and accelerator control rooms a ^3He proportional chamber has been used.

Fission chamber method.
A small ionisation chamber with a thin layer of fissile material (^{235}U) designed by the Section for Instrumentation at AB AtomEnergy Studsvik (Sweden) [28] has been used as an 'on - line' detector both inside and outside the photon beam. The ^{235}U has a high cross section for the thermal neutrons (σ_{ther} = 583 b), about 500 times higher than that for the fast neutrons of energy 1 - 2 MeV.
The pulses from the neutron induced fission products of energies 70 - 100 MeV can

be easily discriminated from the wide spectrum of alpha, beta or gamma ray background, which is always present in the fission chamber. In a mixed neutron - photon beam the pulses generated by neutrons are easy to distinguish from the pulses generated by photons if the frequency of pulses from source is low and the chamber can detect all the pulses separately. At high intensity and highly energetic pulsed photon beams with a low contamination of neutrons, the fission chamber detects primary and secondary photons as well as leptons which contaminate the primary photon beam as one big charge, called PL pulse [9]. The magnitude of this pulse changes with the intensity of the photon beam and is much higher than fission pulses which are always of the same amplitude for given operation parameters of the fission chamber.

In order to measure fast neutrons the fission chamber was put inside a polyethylene cylinder of 15.5 cm diameter and 15.5 cm height. For fast neutron measurements inside the photon beam a special lead block, 3x3x12 cm^3, was applied on the moderator to screen the detector from primary photon and lepton radiation.

The use of this filter decreased the PL to neutron pulse ratio to approximately 10 and improved the pulse counting technique. In these measurements a careful pulse discrimination procedure has been applied to count the neutron contribution to the measured pulse height spectrum and the 'pile-up' effect in the detector has been estimated to be about 10% [9].

The measured values has been corrected for photoneutron production in the lead shield, moderator and detector. The photoneutron production in the lead block and polyethylene moderator for a radiation field of 10x10 cm^2 and a photon energy below 20 MeV is about 4%, for the 21 MeV photons about 7% and for the 42 - 50 MeV photons about 20 -25% of the neutron fluence measured at the detector position. The measured fast neutron fluence has also been reduced by 6% due to thermal neutron diffusion through the moderator.

The measurements outside the primary photon beam were performed without the photon filter. In this region the PL to neutron pulse ratio changed from about 2.5 to 0.05 depending on the scattered photon and lepton background.

The thermal neutron fluence was detected with a bare fission chamber, while the pulse counting technique was the same as for the fast neutrons measurements.

Calibration of the ^{235}U fission chamber.

In order to determine the absolute value of fast neutron fluence inside the treatment room the detector was placed inside the moderator and calibrated using neutrons from a ^{252}Cf source. The calibration procedure was similar to the previous work presented by Gudowska [9].

The thermal neutron fluence conversion factor was taken from earlier studies where

a bare detector was calibrated against thermal neutrons in the isotropic thermal neutron fluence in the SCE pile at the Centre d' Etudes Nucleaires de Grenoble, France [9].

^{3}He chamber method.

Neutron detection by ^{3}He is based on the reaction

$$^3\text{He} + {}^1\text{n} \rightarrow {}^1\text{H} + {}^3\text{H} + 765\ \text{keV} \qquad (2.1)$$

The ^{3}He proportional counter is highly sensitive to thermal neutrons with a cross section of 5400 b and has a low gamma ray sensitivity.
However, this detector cannot be used inside the treatment room due to severe disturbances from the pulsed and intense photon background.
For the measurements outside the treatment room a ^{3}He chamber of 1.2 cm in diameter and the sensitive length of 13 cm manufactured by LMT (Thomson-CFS) has been used.

Calibration of the ^{3}He chamber.
The detector placed inside a polyethylene moderator of 15.5 cm diameter and 15.5 cm height was calibrated using neutrons from a ^{252}Cf source. The geometry of the calibration room and the detector - source distance were similar to that during the calibration of the ^{235}U fission chamber. It was assumed that the moderated neutron spectrum from a ^{252}Cf source at the centre of the polyethylene cylinder is similar to the neutron spectrum outside the treatment room. Since the neutron energy spectrum outside the treatment room of the MM50 racetrack microtron was not studied this assumption may be incorrect and the calibration factor for the ^{3}He chamber may bare a large systematic error. In the future, the Monte Carlo calculations for the neutron transport outside the treatment room and for the neutron transport for the calibration system are planned, that allows the better evaluation of the calibration factor for the ^{3}He chamber.

2.3 Fast and thermal neutron fluence measurements inside and outside the 50 MV photon beam.

Neutron radiation measurements inside the treatment room of the MM50 racetrack microtron, Radiumhemmet, Karolinska Hospital have been performed using the ^{235}U fission chamber. The detector has been placed in the isocenter plane which is horizontal at 1 m SID at different lateral positions from the isocentre as schematically shown in Fig.2.

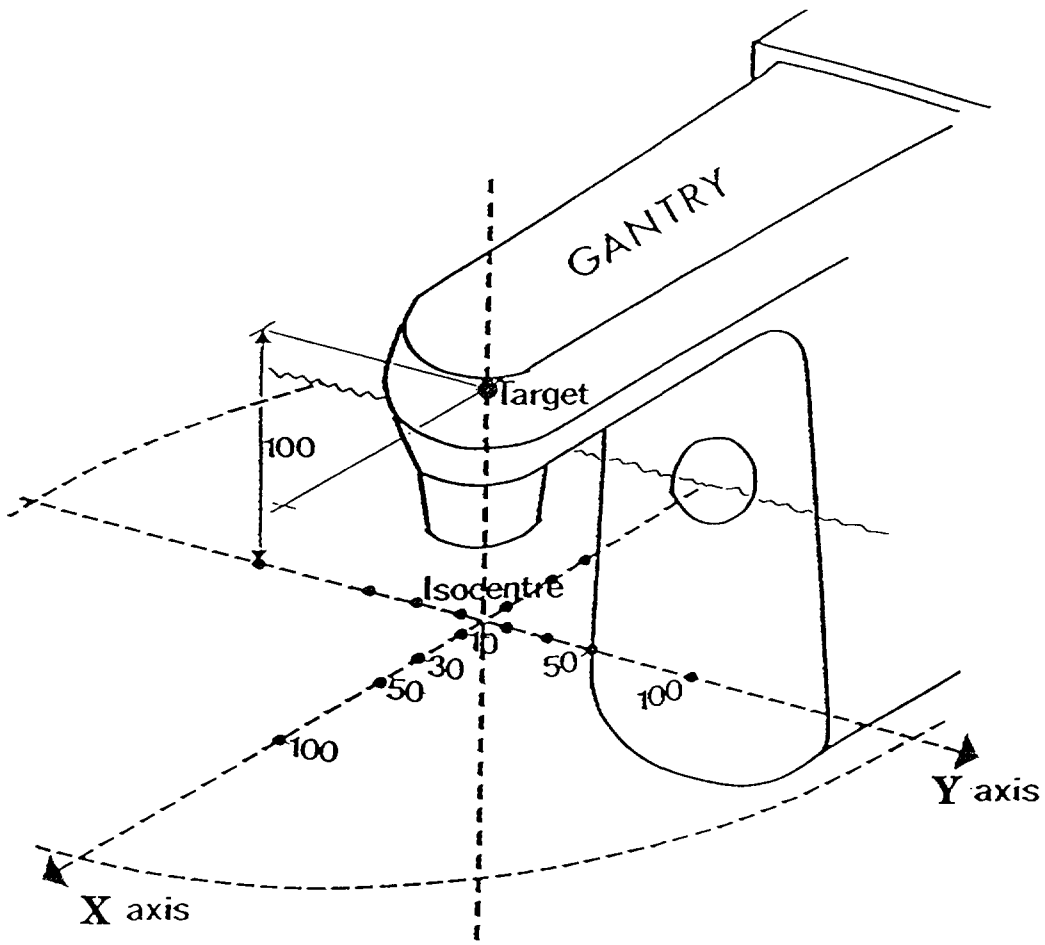

Fig. 2. Geometry used during irradiation and detector positions (in cm) along X - axis (bending plane) and along Y - axis (cross plane).

The fast and thermal neutron fluence profiles along the bending plane axis (X) and perpendicular to it axis (Y) have been measured for a 50 MV photon beam operating in scanned and stationary modes. Different radiation field sizes and two targets: 9 mm Be + 6 mm W (9Be6W) and 5 mm W + 6.5 mm Cu (5.5W6.5W) were used.
Fig. 3 shows the distributions of the fast neutron fluence per unit maximum photon dose in tissue, D_γ, along X and Y axes measured for the 9Be6W target. The similar distributions for the 5.5W6.5Cu target are presented in Fig. 4.

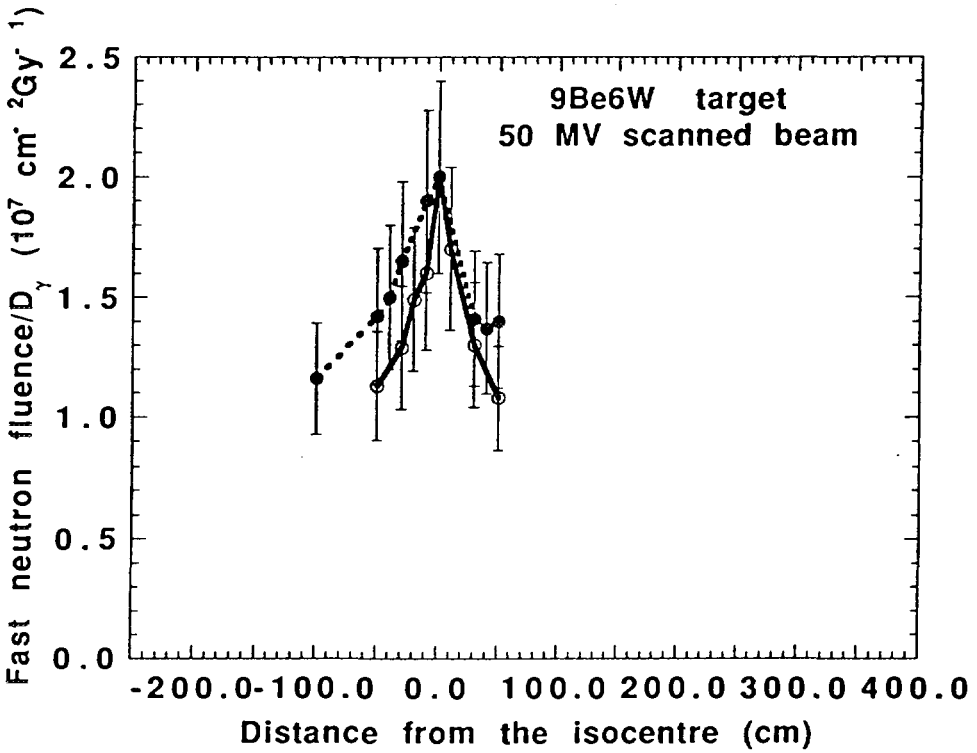

Fig.3. Fast neutron fluence per unit maximum photon dose with the distance from the isocenter (see Fig. 1) for 9Be6W target, X axis - broken line, Y axis - solid line. Field size 10x10 cm^2.

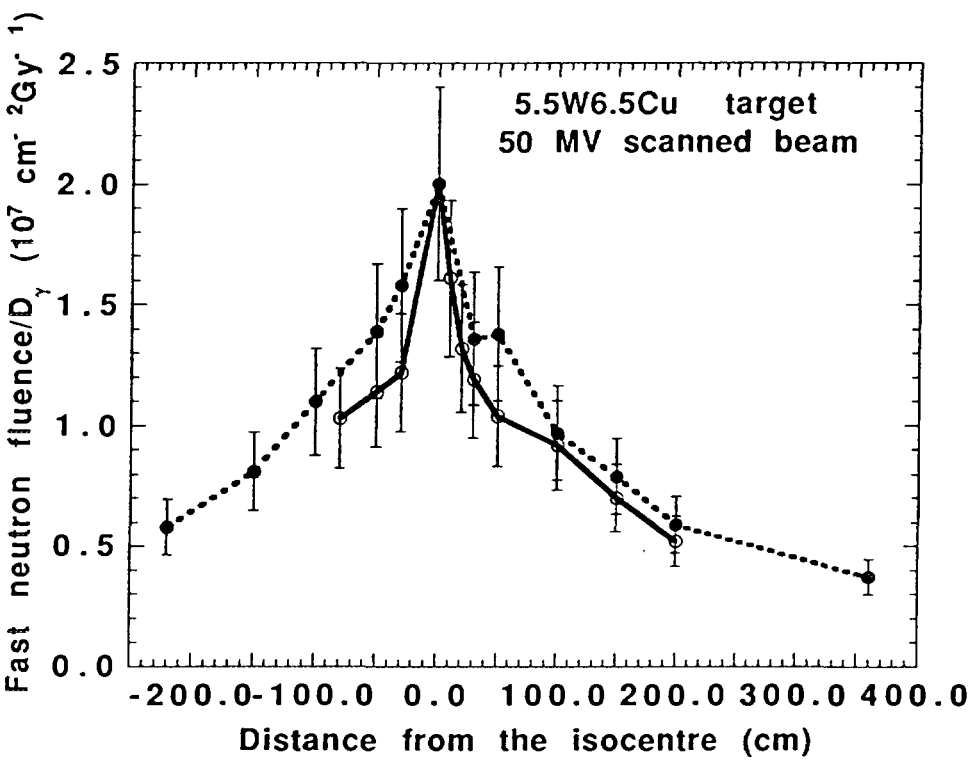

Fig.4. Fast neutron fluence per unit maximum photon dose with the distance from the isocenter for 5.5W6.5Cu target, X axis - broken line, Y axis - solid line. Field size 10x10 cm^2.

The same level of neutron radiation is produced in both targets. The small differences in the shape of these profiles depend mainly on the experimental uncertainty and the level of backscattered neutrons from the walls.
Fig. 5 shows the results of the thermal neutron fluence along X axis normalised to the maximum photon dose measured at isocenter. The thermal neutron fluence inside the central part of the treatment room is almost independent of the distance from the isocentre.
Table I shows the fast neutron fluence per unit maximum photon dose for the stationary and scanned beam modes. The neutron production per maximum photon dose at the isocentre for the 50 MV photon beam and the 9Be6W target is about 4.5 times larger for the scanned mode than for the stationary mode. The scanned photon beam used in this measurement had a circular scanning matrice of 38 cm diameter at 1 m SID. It means that for a radiation field of 10 x 10 cm^2 a larger volume of shielding and collimator materials (Pb, W) in the gantry were irradiated by high energy photons. Not only do the photons produce more neutrons due to this effect but also for a given photon dose at isocenter many more photons are emitted from the target. In consequence a higher neutron radiation level were measured compared to the stationary mode with the unflattened bremsstrahlung beam having a full width at half maximum (FWHM) of 8 cm at 1 m SID [29]. Therefore it is important to only scan as large a field as is needed so the wasted photons don't produce unnecessary neutrons.

The level of the fast neutron fluence inside the therapy room and maze as well as inside the therapy control and the accelerator control rooms is presented in the Table II. The location of the measurement points are shown in Fig. 6. Measurements outside the treatment room have been performed using the ^3He chamber. The level of fast neutron fluence inside the treatment room varies from the 2.0 at the isocentre to 0.1 times 10^7 neutrons cm^{-2} Gy^{-1} near the first shielding door in front of the maze, during operation with 50 MV photons in scanned mode. In the maze, behind the first door, the measured neutron fluence is about 0.002 x 10^7 cm^{-2} Gy^{-1}, whereas outside the maze and behind the second shielding door about half of this value.

The fast and thermal neutron fluences outside the primary photon beam depend strongly on the room design and the constructional materials of the walls and neutron door. The presence of neutron moderating materials in some auxiliary installations in the treatment room decreases the intensity of the fast neutron fluence but increases the level of thermal neutrons since boronated polyethylene was not used.

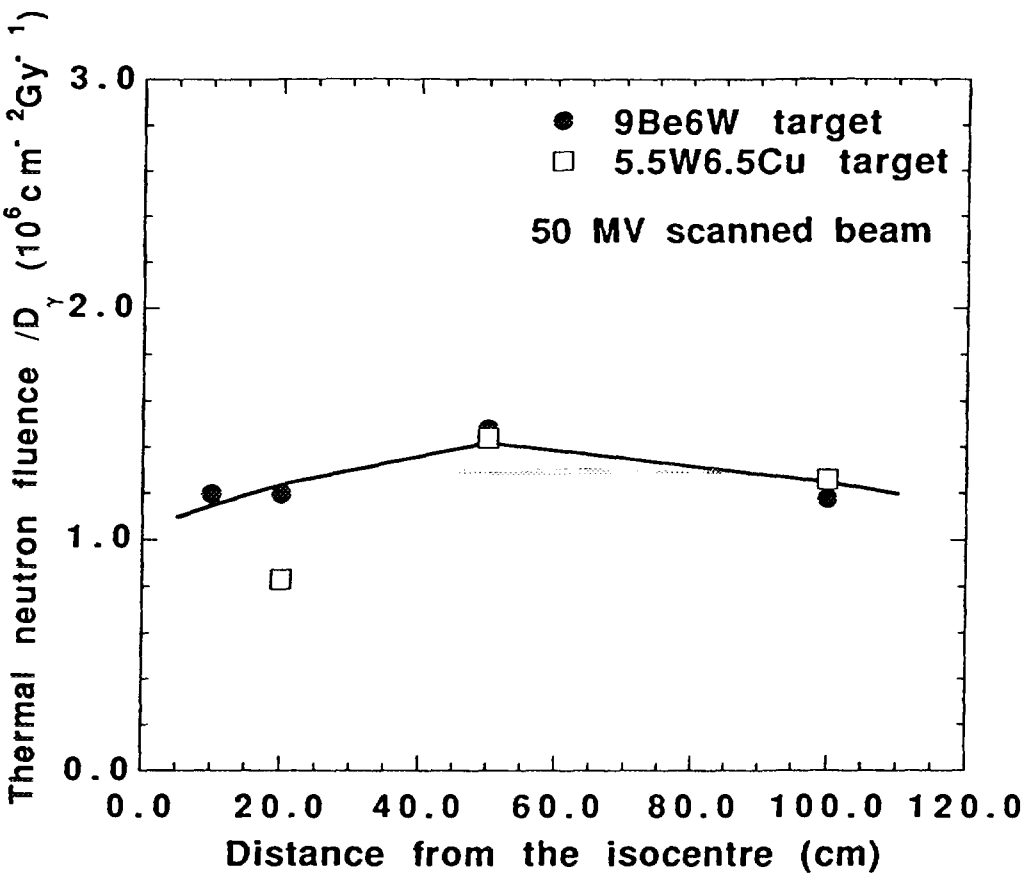

Fig. 5. Thermal neutron fluence per unit maximum photon dose along X axis. Field size 10 x 10 cm^2.

Table I.

Fast neutron fluence per unit maximum photon dose, (cm^{-2} Gy^{-1}), for stationary and scanned beams, 50 MV photons from the MM50 racetrack microtron, two different targets: 9Be6W and 5.5W6.5W, field size 10x10 cm^2.

	Stationary beam		Scanned beam	
	Distance from the isocentre (cm)		Distance from the isocentre (cm)	
Target	0	30	0	30
9Be6W	4.2 x 10^6	2.2 x 10^6	2.0 x 10^7	1.3 x 10^7
5.5W6.5Cu	4.6 x 10^6	3.3 x 10^6	2.0 x 10^7	1.2 x 10^7

Table II.

Neutron radiation around the MM50 racetrack microtron measured using the ^{235}U and ^{3}He chambers.

See Fig. 6 for the detector position. Positions 1 and 2 refer to 0 and 100 cm from the isocentre, respectively. The results for the positions 1 - 6 are related to the fast neutron fluence measurements, whereas the positions 7 - 18 (in the maze and outside the treatment room) are related to neutron fluence measurements for the moderated neutron spectrum.

The same electron current was used for the bremsstrahlung beam and the electron beam stopped in the wall (pos. S). For the latter case the measured fast neutron fluence rate at the positions 12 - 18 was normalised to the corresponding photon dose rate at dose maximum (0.21 Gy/min) when bremsstrahlung beam is produced in the 9Be6W target.

Operation mode	50 MV photons, 9Be6W target, scanned beam, field 10 x 10 cm^2											50 MeV electron beam stopped in the wall (pos. S)						
Measurement method	^{235}U chamber							^{3}He chamber				^{3}He chamber						
Position	1	2	3	4	5	6	7	8	9	10	11	12	13	14	15	16	17	18
Neutron fluence per maximum photon dose (cm^{-2} Gy^{-1})	$2.0\ 10^7$	$9.2\ 10^6$	$4.5\ 10^6$	$2.8\ 10^6$	$2.6\ 10^6$	$1.0\ 10^6$	$2.0\ 10^4$	$9.5\ 10^3$	$5.4\ 10^3$	$0.5\ 10^3$	$0.3\ 10^3$	$2.9\ 10^1$	$1.1\ 10^2$	$1.7\ 10^2$	$2.9\ 10^2$	$2.6\ 10^2$	$8.6\ 10^1$	$5.1\ 10^2$

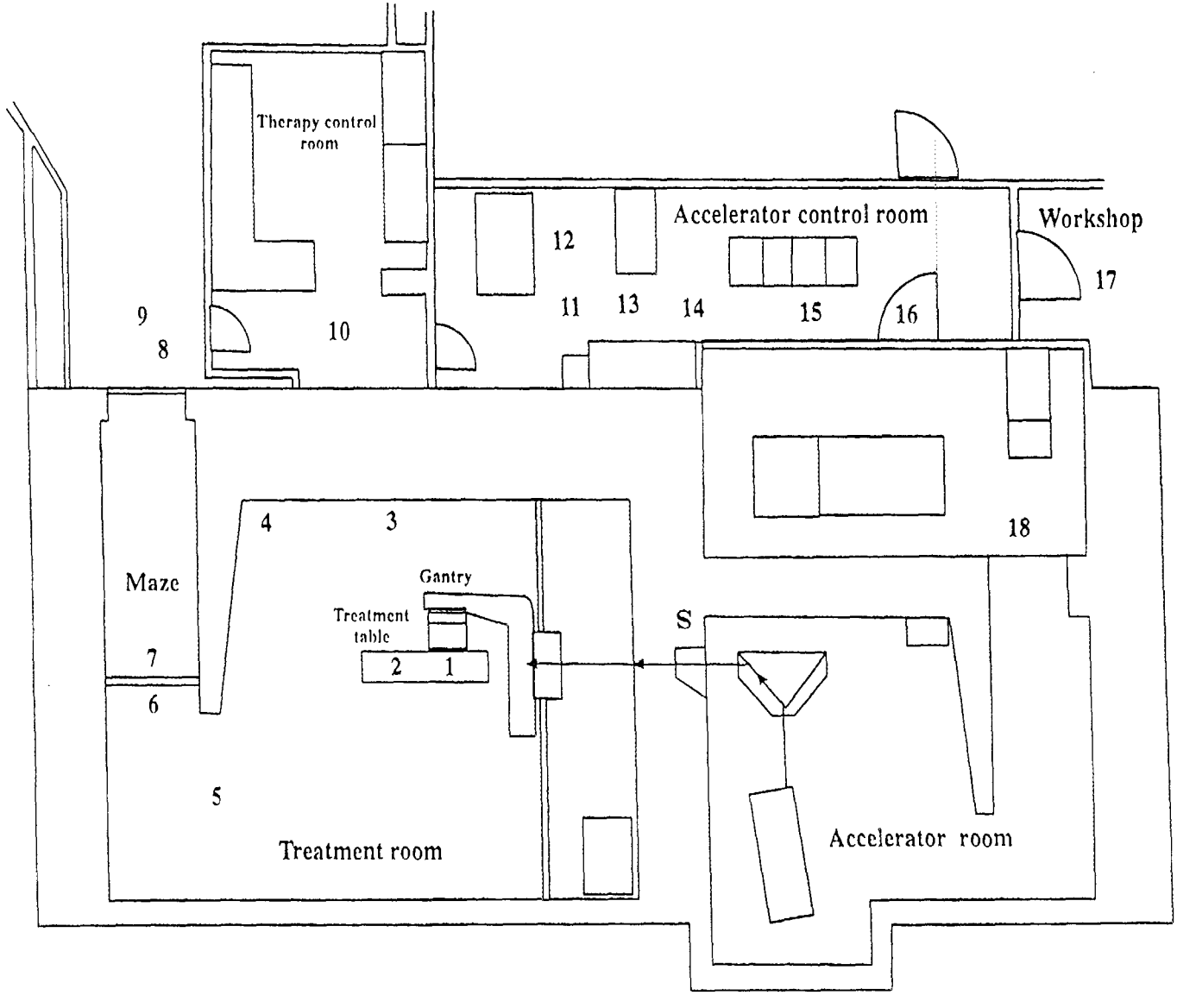

Fig. 6. Schematic drawing of the treatment room, maze, therapy and accelerator control rooms, and accelerator room of the MM50 Racetrack microtron at Radiumhemmet, Karolinska Hospital.
Numbers show the position of detectors used for neutron fluence measurements.

2.4 Fast neutron fluence measurements in scanned bremsstrahlung beams in the range 10 - 50 MV.

The fast neutron fluences at the isocentre have been determined for a wide range of the operating electron energies from 10 up to 50 MeV for the 9Be6W target and the scanned mode.

Fig. 7 shows the fast neutron fluence as a function of the maximum photon energy in the 10 - 50 MV bremsstrahlung beams for the measurement points 0 and and 30 cm from the isocentre .

The neutron production is increasing with the acceleration energy up to 30 MV. Between 30 and 50 MV a constant neutron yield is observed at the measurement point 30 cm from the isocentre. At the isocentre, the neutron production reaches maximum for the 35 MV photon bremsstrahlung beam, whereas a slight decrease is observed for the higher energies up to 50 MV.

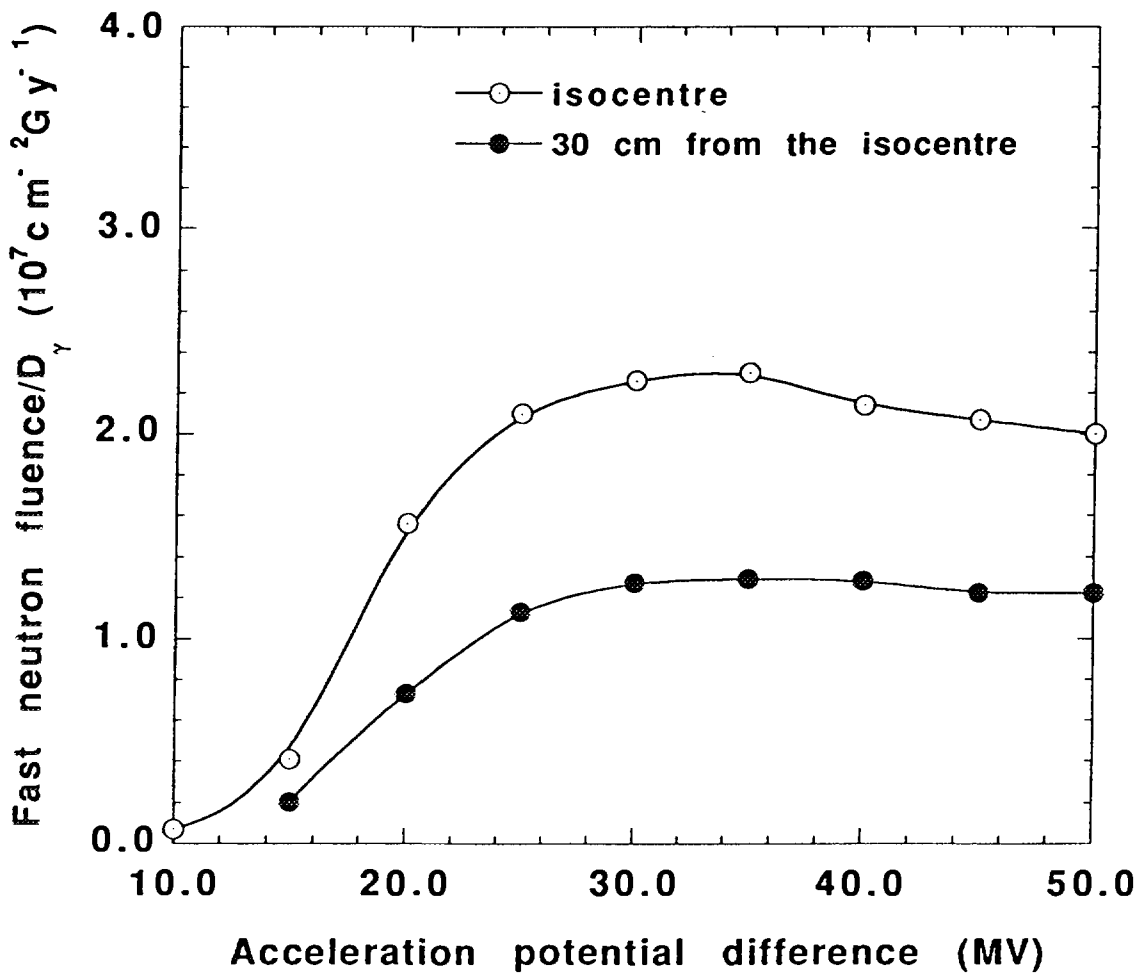

Fig. 7. Fast neutron fluence per unit maximum photon dose as a function of the maximum photon energy for the 10 - 50 MV bremsstrahlung beams .

2.5 Discussion.

The fast neutron fluence profile from eight medical electron accelerators at different hospitals in Sweden and the 50 MeV electron accelerator at the Department of Accelerator Technology at the Royal Institute of Technology (RIT) are compared in Fig. 8. The fast neutron fluence and absorbed dose to tissue are normalised to the maximum photon dose in tissue and the distributions presented are along the X axis.

The neutron absorbed dose in tissue was calculated using the fluence-to-absorbed dose conversion factors from NCRP Report 79 [1]. The fluence-to-absorbed dose conversion factors as a function of a mean energy of photoneutrons as given in NCRP Report 79 were evaluated by averaging the data for monoenergetic neutrons from ICRP Publication 21 [30] over the photoneutron spectra from medical electron accelerators [31]. In the latter publication the conversion factors were calculated for a broad beam of monoenergetic neutrons impinging on a 30 cm thick slab of the soft tissue material and for the depth of maximum dose equivalent. For neutrons from medical electron accelerators (mean energy 0.5 - 1.0 MeV) these factors are for a depth of about 1 cm in the soft tissue.

The absorbed dose in tissue due to fast neutrons for the 40 - 50 MV units was calculated using the fluence-to-absorbed dose conversion factor of 4.5×10^{10} cm^{-2} Gy^{-1} [1], assuming a neutron spectrum with a mean energy of 1 MeV [2]. For the 16 - 21 MV units a conversion factor of 5.8×10^{10} cm^{-2} Gy^{-1} [1] was used for the photoneutron spectrum assuming a mean energy of 0.6 MeV [3,4].

The treatment units in the energy range 16 - 42 MV were operating with stationary beams using conventional flattening filters. Two racetrack microtrons (MM50, Scanditronix) at the Karolinska Hospital in Stockholm and the University Hospital in Umeå were operating with a beam scanning system whereas results from the 50 MV racetrack from the accelerator laboratory at RIT pertain to an unfiltered stationary beam.

The photoneutron production in the 16 - 21 MV units is generally higher, by a factor of about 1.2 - 2.0, than that for the 40 - 50 MV machines. These differences are mostly due to differences in the design of the treatment head, especially because of the absence of the thick flattening filters in modern high energy photon machines. In addition the normalisation to the photon absorbed dose at the depth of the dose maximum results in a lower photoneutron production in the 40 - 50 MV range because of the lower photon fluence required to produce a photon dose of 1 Gy. This is due to the fact that the gross photoneutron production is almost independent of photon energy above 25 MV.

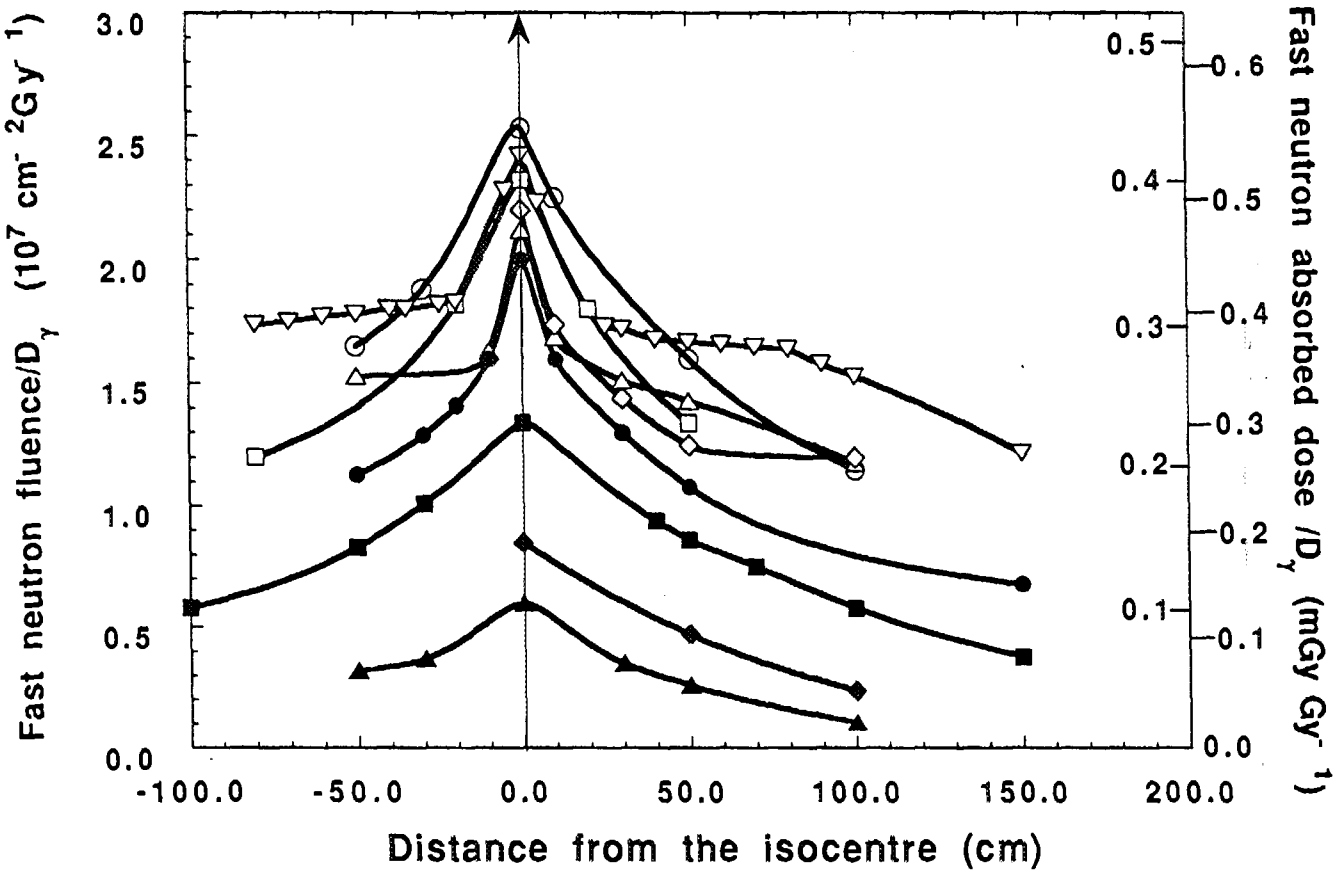

Fig. 8. Fast neutron fluence and absorbed dose in tissue normalised to the maximum photon dose at the isocentre. The left and right scales on the right axis correspond to absorbed dose values for the 16 - 21 MV and 40 - 50 MV units, respectively. X - axis, 10 x 10 cm^2 field size, 1 m SID. All results except for 50 MV Racetrack Microtron, KS are taken from Gudowska [9].

Key: (△) 16 MV Philips (In foil, Uppsala), (□) 18 MV Philips (fiss. cham., Lund), (○) 18 MV Saturne (fiss. cham., Örebro), (◇) 21 MV Microtron (fiss. cham., Stockholm), (▽) 21 MV Microtron (fiss. cham., Umeå), (▲) 42 MV Siemens Betatron (fiss. cham., Malmö), (■) 50 MV Racetrack Microtron (fiss. cham., Umeå), (●) 50 MV Racetrack Microtron (fiss. cham., Stockholm, KS), (◆) 50 MV Racetrack Microtron . (fiss. cham., Stockholm, RIT) .

The neutron fluence at isocentre for the 50 MV Racetrack microtron in Stockholm is about 50% higher than that for the machine in Umeå. Both facilities are located in treatment rooms of similar size. A thick target of 9mm Be and 6mm W was employed for the racetrack in Stockholm, whereas the target at the racetrack in Umeå consisted of a thin target of 1.6 mm Ta and a 10 cm thick graphite electron stopper. No flattening filter was used in either machine and they were operating in the scanning beam mode with the similar circular scanning pattern of a radius 20 cm at 1 m SID. For the radiation field size of 10 x 10 cm^2 it implies that the high energy photons were directed over a large volume of shielding material (W, Pb and Fe) in the gantry resulting in the higher photoneutron production when compared to a more clinically relevant patient individual scanning pattern. In this case mainly the difference in target design explains the different photoneutron production inside and outside the primary photon beams.
The 50 MV racetrack microtron placed at the accelerator laboratory (RIT) is operated in the stationary beam mode and thus generates the lowest photoneutron contamination. A very simple construction of the accelerator head and 1.5mm thin Ta target with an aluminium electron stopper (11 cm), a very thin (0.1mm) Pb electron scattering foil and a simplified collimator built of only a few lead blocks reduced significantly the photoneutron radiation measured at a distance of 100cm from the target.
The 42 MV Siemens Betatron in Malmö with the very thin target and thin flattening filter of Pb shows the lowest level of the photoneutron radiation. In this case the neutron fluence at isocentre was reduced further due to the negligible contribution from wall scattered neutrons because of a very large therapy room.

The statistical error of the measured neutron fluence using the ^{235}U chamber is about 12% on the one sigma level taking errors of the fission fragment pulse counting, the noise of the electronic system, fluctuations of the photon dose rate during the measurements and statistical errors during the calibration procedure into account [9].
In these investigations the filtered neutron spectra inside the treatment room of the therapy units was not studied in detail. Only a rough estimate of the mean neutron energy was done based on the studies by Nordell [2] and McCall [3] for medical electron accelerators of similar maximum electron energy. The fast neutron fluences inside the treatment room determined by the calibration procedure with a ^{252}Cf source bare therefore a systematic error of about 10 -15 %.
The total error of the fast neutron fluence measurements is about 20% (1σ).
On the other hand the neutron absorbed dose calculated using the measured neutron fluence and the fluence-to-absorbed dose conversion factor from NCRP

Report 79 bares an additional systematic error about 10 - 15 % due to uncertainty of the average energy of the photoneutron spectrum.
However, assuming an absolute accuracy of the determined neutron fluence or absorbed dose levels of about 20 - 25 % sufficient for the radiation protection purposes, the detection methods employed such as foil activation or ^{235}U fission chamber and the calibration procedure for the neutron fluence from the ^{252}Cf source are satisfactory.

3. Computer simulation of neutron sources, neutron transport and neutron fluence inside the treatment room of a MM50 racetrack microtron.

3.1 Determination of the bremsstrahlung spectrum using the ITS 3.0 code.

The Monte Carlo code ITS 3.0 [32] has been used for electron transport, bremsstrahlung production and photon transport calculations for a 50 MeV scanned electron beam impinging on the 9Be6W target. Due to bugs in the ITS 3.0 code for the oblique beams the calculation of the bremsstrahlung spectrum was made for a pencil beam, impinging perpendicularly on the target. A simplified geometry of the target and shielding blocks of lead has been used in the photon transport calculations. All parts of the treatment head were assumed to be the cylindrical bodies with the axes along the central axis of the treatment head. This assumption is not excactly correct for some part of the collimators and shielding blocks. A correction for the obliquity of the scanned beam, approximately acounting for the true photon trajectories in the treatment head was also made. Similar approximation was also done for the photon transport in the tungsten collimators. Because of this simple approach, the calculated photon energy spectra in the cells of the treatment head are therefore approximate and bare uncertainty which also affects the calculated photonuclear energy spectra.

3.2 Determination of the photoneutron sources inside the treatment head.

The photoneutron sources have been determined analytically for the cells in the W target, W collimators and Pb shielding blocks, since mainly these materials contribute to the photoneutron production inside the treatment head.
Neutrons produced by the photonuclear reactions in the heavy materials (W, Pb) originate from two main mechanisms: evaporation and direct processes [1].
The energy spectrum of photoneutrons for a heavy nuclide, averaged over the unit volume is considered as:

$$Y(E_n)\,dE_n = c_{ev}\,Y_{ev}(E_n)\,dE_n + c_{dir}\,Y_{dir}(E_n)\,dE_n \qquad (3.1)$$

where the first and second terms are the evaporation and direct components, respectively. E_n is the neutron energy, c_{ev} and c_{dir} are two constants taking into account that the number of the photoneutrons produced due to direct process is assumed to be 12% of the photoneutrons produced in the evaporation process [1].

The energy distribution of photoneutrons from the evaporation process can be

described by the statistical model developed by Weisskopf [33] and expressed by the Maxellian form as:

$$c_{ev}\, Y_{ev}(E_n)\, dE_n = C\,(0.893/T^2)\, E_n \exp(-E_n/T)\, dE_n \qquad (3.2)$$

where C ($C = \int Y(E_n)\, dE_n$) is the total number of photoneutrons produced in the unit volume and the constant T is the nuclear temperature. The nuclear temperature is a measure of the excitation of the product nucleus after the emission of neutron and is assumed to be independent of the neutron energy when the neutron energy is much smaller than the photon excitation energy. In this calculation the nuclear temperatures of 1.0 and 0.5 MeV for Pb and W, respectively [1] were applied.

The direct component is given by:

$$c_{dir}\, Y_{dir}(E_n)\, dE_n = 0.107\, \sigma_{\gamma,xn}(E_\gamma)\, \Phi_\gamma(E_\gamma)\, dE_n \qquad (3.3)$$

where:

$E_n = E_\gamma - E_t$ [MeV]

E_t [MeV]	is the threshold energy for the photonuclear reaction,
$\sigma_{\gamma,xn}(E_\gamma)$ [m^2]	is the cross section for the photonuclear reaction at photon energy E_γ,
$\Phi_\gamma(E_\gamma)dE_\gamma$ [m^{-2}]	is the fluence of photons in the energy interval E_γ, $E_\gamma + dE_\gamma$ obtained from the ITS 3.0 calculations.

From $E_n = E_\gamma - E_t$ it follows that $dE_n = dE_\gamma$.

The cross sections for the photonuclear reactions in Pb and W have been taken from Dietrich and Berman [34].

Fig. 9 shows a cross section of the treatment head with the neutron source cells as coded in the analytical calculation and neutron transport simulation using the MCNP4A code [35]. Totally 30 neutron source cells have been determined with the neutron energy distribution described by the equations (3.1 - 3.3).

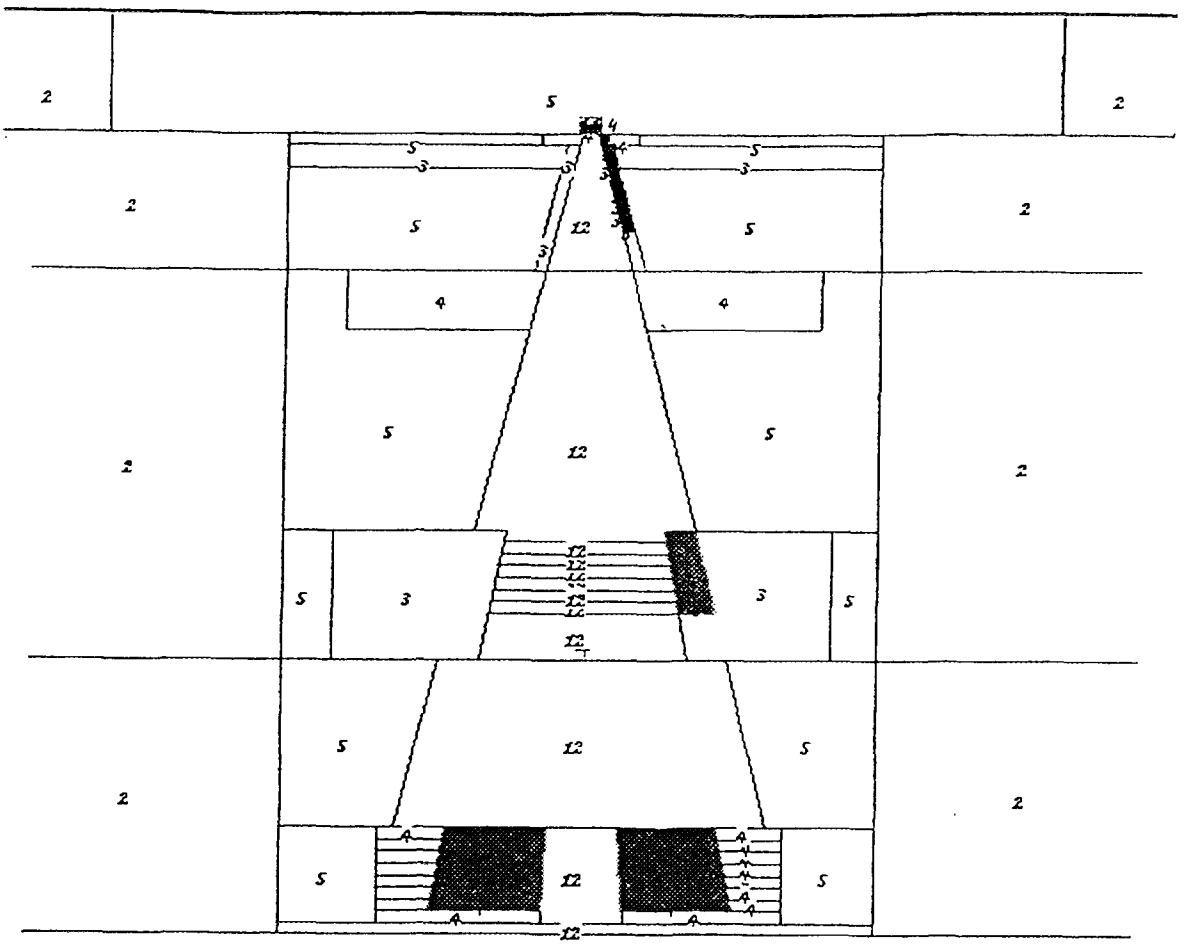

Fig. 9. A cross section view of the treatment head. The black coloured cells are the neutron source cells of the total number of 30. Numbers are related to the material used in the treatment head. Material: 2 - air, 3 - lead, 4 - tungsten, 5 - iron, 12 - He gas.

3.3 Calculation of the photoneutron transport and neutron fluence inside the treatment room by the Monte Carlo code MCNP4A.

Computer simulation of photoneutron transport inside the treatment room of the MM50 racetrack microtron at KS, have been performed using the Monte Carlo code MCNP4A [35]. Neutron transport calculations with the neutron sources defined in the treatment head (see Fig. 9) have been done for the entire treatment room and maze geometry, shown on Fig. 10. Totally 101 cells have been defined for neutron transport in the treatment room and maze with the wall and door materials of concrete, iron-concrete, gypsum and polyethylene.

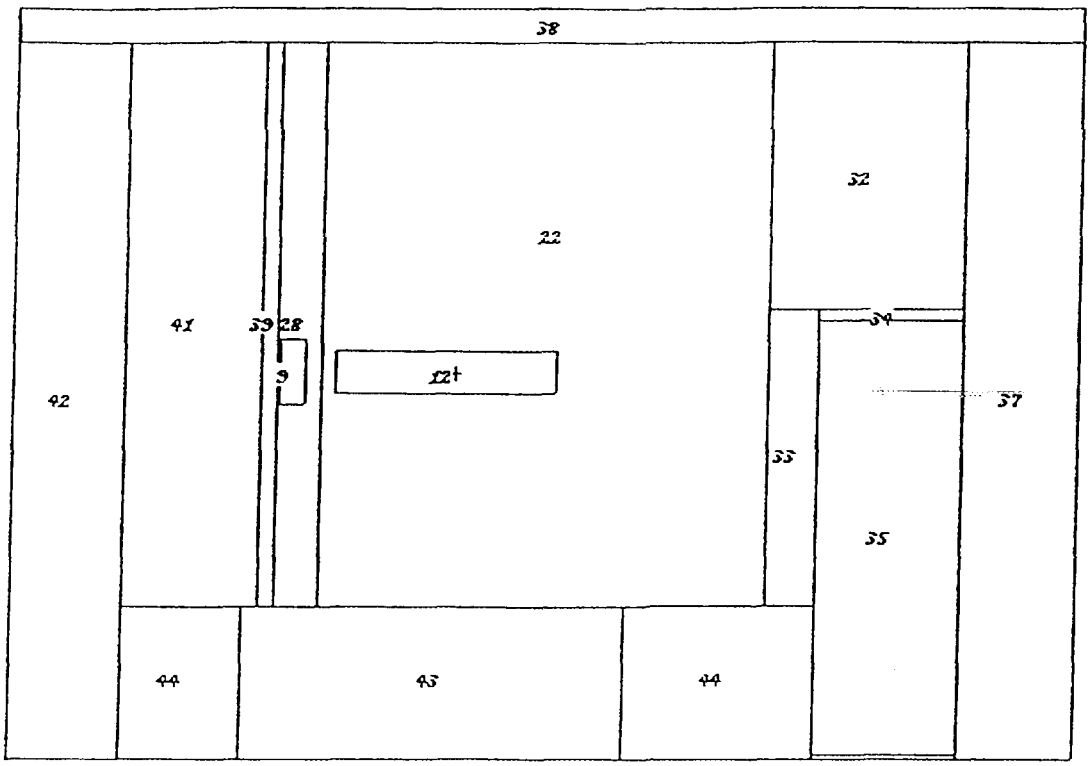

Fig. 10. The cross section view through the treatment room of the MM50 racetrack microtron in the plane parallel to the treatment table and at the distance 1m SID as coded in the simulation using the MCNP4A code. The wall cells: 33, 37, 38, 42, 44 - concrete, wall cell 43 - iron-concrete, wall cell 39 - gypsum, treatment room cells: 22, 28, 41, 32 - air, gantry cell 9 - iron, treatment table cell 12 - iron, accelerator door cell 34 - polyethylene, maze cell 35 - air.

The fast neutron fluences have been calculated at the isocenter and for the positions 10, 30, 50, 100 and 150 cm from the isocenter in a plane parallel to the treatment table at 1 m SID (source-isocenter-distance). Fig. 11 shows the positions (1 - 6) for the calculated neutron fluences.

The calculated fast neutron fluences have been normalised to maximum photon dose evaluated for the tissue equivalent phantom of 30 cm thick slab using the 50 MV bremsstrahlung spectrum from computer simulation by ITS 3.0.

Table III shows the calculated fast neutron fluences per maximum photon dose and the measured data recorded at the same points for the same operation mode of the 50MM racetrack microtron at KS. The calculated fluences are about from 3.5 to 1.5 times larger than the experimental results depending of the distance from the isocenter.

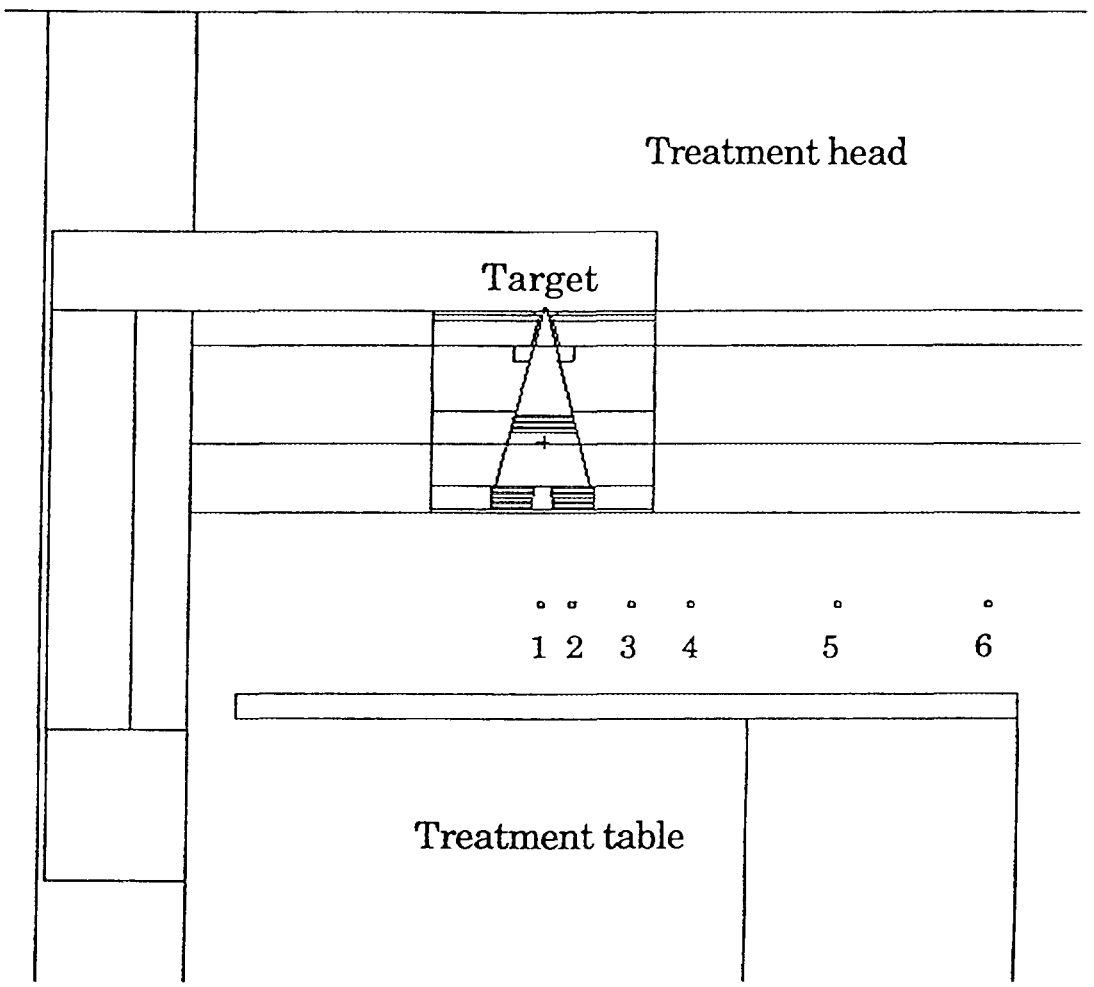

Fig. 11. The cross section view of the treatment head in the bending plane of the gantry, as coded in the simulation using the MCNP4A code. The positions 1 - 6 are at the distances 0, 10, 30, 50, 100 and 150 cm from the isocenter in the patient plane at 1 m SID.

Table III.
The accelerator produced fast neutron fluence per maximum photon dose, 10^7 (cm^{-2} Gy^{-1}) calculated by computer simulation using the MCNP4A code and measured using the ^{235}U fission chamber method. 50 MV photons from the MM50 racetrack microtron, scanned beam, field 10x10 cm^2, target 9Be6W. Positions 1 - 6 are at the distances 0, 10, 30, 50, 100 and 150 cm from the isocenter in the patient plane at 1 m SID.

Position	1	2	3	4	5	6
Distance from the isocenter (cm)	(0)	(10)	(30)	(50)	(100)	(150)
Calculated results	7.0	4.0	2.7	1.8	1.2	1.5
Measured results	2.0	1.6	1.3	1.1	1.0	0.8

The error of fast neutron fluence measured using the ^{235}U fission chamber method is about 20% (1σ) (see sec. 2.5). The statistical error of the Monte Carlo simulation of bremsstrahlung spectrum by ITS 3.0 is about 2% (1 σ) for the calculation with 10 000 histories. The statistical error of the simulation of neutron fluences using MCNP4A is about 8% (1σ) for the 700 000 histories. The systematic error due to uncertainty of the photoneutron cross section data is about 5 - 15% [34] depending on the photon energy and the systematic error due to calculation of maximum photon dose about 10%. The total calculation error taking into account mentioned above factors is about 20% (1σ). Additionally, the systematic error due to simplified geometry of the treatment head and assumption for the approximate photon trajectories in the oblique beam geometry should be added. The latter error largely affects the uncertainty of the determined photon fluences and hence the neutron sources in the cells, and is probably the main reason for a discrepancy between the calculated and measured fast neutron fluences.

3.4 Discussion.

Evaluation of the photoneutron fluence inside the treatment room were performed in three separate calculation steps: 1) calculation of the bremsstrahlung spectrum inside the treatment head using ITS 3.0, 2) analytical evaluation of the photoneutron sources, and 3) simulation of the neutron transport and calculation of the fast neutron fluence using MCNP4A. Using analytical calculations (step 2) the energy distribution of the produced photoparticles both from evaporation and direct processes is determined in order to specify the neutron sources for MCNP4A.
In the first step the description of the treatment head geometry was simplified and due to bugs in the ITS 3.0 code photon transport evaluated for the electron beam impinging perpendicularly on the target instead for the oblique geometry of the scanned beam. Next, a geometrical correction for the true photon trajectories has been done. Using this method the calculation time was increased and resulted in a large systematic uncertainty of the photon energy spectra due to treatment of the irradiation geometry. In consequence the evaluation of the photoneutron sources in the cells was less accurate. In the third step neutron transport simulation by MCNP4A were performed for the well defined geometry of the treatment head and the treatment room.
The calculated fast neutron fluences in the patient plane (Table III) differ from 1.5 to 3 times from the measured data. This discrepancy is probably mainly due to inaccurate description of the geometry for photon transport in the treatment head.

Since the evaluation of the photoneutron fluences inside the treatment room using this approach was too approximative it would be useful to improve the calculation method by using the latest version of the MCNP code, MCNP4B or the FLUKA 93/94 code [36].
In MCNP4B the ITS 3.0 algorithm has been implemented for electron and photon transport mode. It means that using MCNP4B the geometry of the treatment head and room can be defined in the same way for electron, photon and neutron transport. That makes the evaluation of neutron sources in the cells more correct and more simple. Additionally, in MCNP4B the problem of describing the oblique beam geometry is eliminated. Still, using this method the evaluation of the photoneutron energy spectra has to be done analytically, since in MCNP4B the photoneutron processes are not included.
On the other hand in FLUKA 93/94 transport of electrons, photons and photonuclear particles is followed in one package, that makes this code an attractive tool to evaluate photon and neutron radiation around high energy medical electron accelerators.

4. Determination of the absorbed dose in tissue due to photonuclear reactions during radiation therapy with a 50 MV bremsstrahlung beam.

4.1 Cross section for photonuclear reactions in tissue equivalent materials.

For the light nuclei (A < 40) the nuclear absorption of x-rays in the energy range 5 - 25 MeV takes mainly place through the excitation of the nucleus and emission of a single particle [37]. The collective vibrations between the protons and neutrons initiated by the photon excitation process lead to a collective resonance called the giant dipole resonance. For intermediate energy photons the giant resonance dominates the photon absorption cross section in nuclei. For energies above the giant resonance the most important absorption mechanism is through the interaction with a pair of nucleons (n - p cluster) inside the nucleus. In either case the excited photonuclear particles emerge directly without further interaction, and their energy and angular distributions reflect the absorption process. For light nuclei a characteristic structure of the giant resonances for each element is observed, revealing the individual structure of the nuclear levels.

High energy photons in the energy range from a few MeV up to 60 MeV interact with light elements in tissue to produce high LET particles such as neutrons, protons, alphas, ^{3}He and deuterium particles depending on the photon energy.

In the energy region of the giant resonance the photoneutron and photoproton reactions are the dominat photonuclear processes in the light nuclei with the (γ, n) and (γ, p) cross sections similar in magnitude and shape [38]. At energies above the giant resonace the most important absorption mechanism is through the quasideuteron effect where a neutron - proton pair emerge from the nucleus with energy and angular correlation appropriate to the photodisintegration of a deuteron.

The cross section for the production of heavier photonuclear particles like alpha, ^{3}He and deuterons is much lower than the cross sections for (γ, n) and (γ, p) reactions and scarcely discussed in the literature. In oxygen and carbon the photonuclear cross section for production of these particles contribute less than 2% to the integral of the total photonuclear absorption cross section up to 30 MeV [38]. However, the contribution by alphas and ^{3}He to the total photonuclear dose delivered to tissue may be biologically signifficant (also at low particle fluences) due to the high LET of these heavier particles. The radiobiological effect of these particles are characterised by a RBE value which is significantly higher than unity and they may be of high importance.

In the present work the absorbed dose delivered to a tissue equivalent (TE)

phantom due to photonuclear reactions was calculated for a scanned photon beam of 50 MV produced by the 9Be6W target of the racetrack microtron at the Karolinska Hospital.

The elemental composition of the phantom material was assumed to be an average soft tissue in an adult male [39] (fraction by weight) : 0.105 H, 0.256 C, 0.027 N, 0.602 O, 0.001 Na, 0.002 P, 0.003 S, 0.002 Cl, 0.002 K.

A list of the main photonuclear reactions in elements of an average soft tissue used in the evaluation of the photonuclear dose is shown in Table IVa,b,c. The integrated cross sections for photonuclear particle production in (n, p, α, ^{3}He etc.) tissue are also presented. The photonuclear cross section data were taken from Fuller [38] and Vessière et al [40].

Oxygen, carbon and nitrogen are the main nuclei for neutron and proton production in the tissue. The rarer elements ^{18}O , ^{13}C, ^{15}N, ^{23}Na, ^{nat}Cl, ^{31}P, ^{32}S, ^{39}K are responsible for less than 2% of the produced neutrons and protons. ^{4}He, ^{3}He and ^{2}H particles are produced mainly in oxygen and carbon.

The variation of photonuclear cross section for neutron, proton, ^{4}He, ^{3}He and deuteron production in an average soft tissue is shown in Fig. 12. The photoneutron cross sections for the constituent elements of human tissues were taken from Fuller [38] and Vessière et al [40] and weighted for the relative contribution of each element to the total photonuclear cross section. The peaks of the photonuclear cross section for neutron and proton production in the tissue are in the photon energy range 20 - 40 MeV. A significant alpha production is observed for photons of energies 13 - 36 MeV. ^{3}He and deuterium particles with the cross section yields about 10 times lower than for alpha particles are expected to be produced by photons of energies 24 - 30 MeV.

TABLE IVa.

Photonuclear reactions in a soft tissue (adult male ICRU-44, ICRU 1989) of the elemental composition (fraction by weight) : 0.105 H, 0.256 C, 0.027 N, 0.602 O, 0.001 Na, 0.002 P, 0.003 S, 0.002 Cl, 0.002 K, density 1.03 g/cm^3.

$\int\sigma_S$ dE (MeV mb) is the integrated cross section for photonuclear production of s - particle (n, p, α, ^{3}He, etc.) integrated from the threshold energy for the (γ, xs) reaction to the maximum bremsstrahlung energy, here 50 MeV.

(γ,n*$_{5.2}$) is related to the excited-state transition reaction (γ,n*) with the excitation energy of 5.2 MeV.

Element	^{16}O	^{12}C	^{14}N	^{18}O	^{13}C	^{15}N	^{23}Na	^{nat}Cl	^{31}P	^{32}S	^{39}K
Atomic fraction in tissue	0.22585	0.12685	0.01152	0.00040	0.00132	0.00004	0.00060	0.00033	0.00056	0.00054	0.00029
(γ, xn) reactions	(γ,n$_0$) (γ,n*$_{5.2}$) (γ,n*$_{6.18}$) (γ,n*$_{6.79}$) (γ,np)	(γ,n$_0$) (γ,n*$_{2.0}$) (γ,n*$_{4.0}$)	(γ,n$_0$) (γ,np*$_{3.5}$)	(γ,n) (γ,2n)	(γ,n) (γ,2n)	(γ,n) (γ,np) (γ,2n)	(γ,n) (γ,2n) (γ,np)	(γ,n) (γ,2n) (γ,np)	(γ,n) (γ,np)	(γ,n) (γ,np)	(γ,n) (γ,np)
$\int\sigma_n$ dE (MeV mb)	103.5	62.8	113.0	198.2	126.0	105.9	137.0	294.4	182.0	98.0	210.0
$\int\sigma_n$ dE weighted by atomic fraction (MeV mb)	23.375	7.966	1.302	0.080	0.166	0.004	0.083	0.097	0.103	0.053	0.060

TABLE IVb.

Element	^{16}O	^{12}C	^{14}N	^{18}O	^{13}C	^{15}N	^{23}Na	^{nat}Cl	^{31}P	^{32}S	^{39}K
(γ, xp) reactions	(γ,p_0) (γ,$p^*_{5.3}$) (γ,$p^*_{6.33}$) (γ,$p^*_{7.3}$) (γ,np)	(γ,p_0) (γ,$p^*_{2.1}$) (γ,$p^*_{5.0}$)	(γ,p_0) (γ,$np^*_{3.5}$) (γ,$p^*_{3.7}$) (γ,$p^*_{7.7}$)	(γ,p)	(γ,p)	(γ,p)			(γ,np)	(γ,np)	(γ,np)
$\int\sigma_p$ dE (MeV mb)	177.4	80.3	25.2	44.4	36.0	70.0			50.0	18.1	60.0
$\int\sigma_p$ dE weighted by atomic fraction (MeV mb)	40.066	10.186	0.290	0.018	0.047	0.003			0.028	0.010	0.017
(γ, xα) reactions	(γ,α_0) (γ, 4α)	(γ, 3α)									
$\int\sigma_\alpha$ dE (MeV mb)	5.88	2.96									
$\int\sigma_\alpha$ dE weighted by atomic fraction (MeV mb)	1.328	0.375									

TABLE IVc.

Element	^{16}O	^{12}C	^{14}N	^{18}O	^{13}C	^{15}N	^{23}Na	^{nat}Cl	^{31}P	^{32}S	^{39}K
(γ, ^{3}He) reactions	(γ, ^{3}He)	(γ, ^{3}He)	(γ, ^{3}He)								
$\int\sigma_{^3He}$ dE (MeV mb)	0.741	1.14	0.259								
$\int\sigma_{^3He}$ dE weighted by atomic fraction (MeV mb)	0.167	0.145	0.003								
(γ, d) reactions	(γ,d_o)										
$\int\sigma_d$ dE (MeV mb)	0.402										
$\int\sigma_d$ dE weighted by atomic fraction (MeV mb)	0.091										

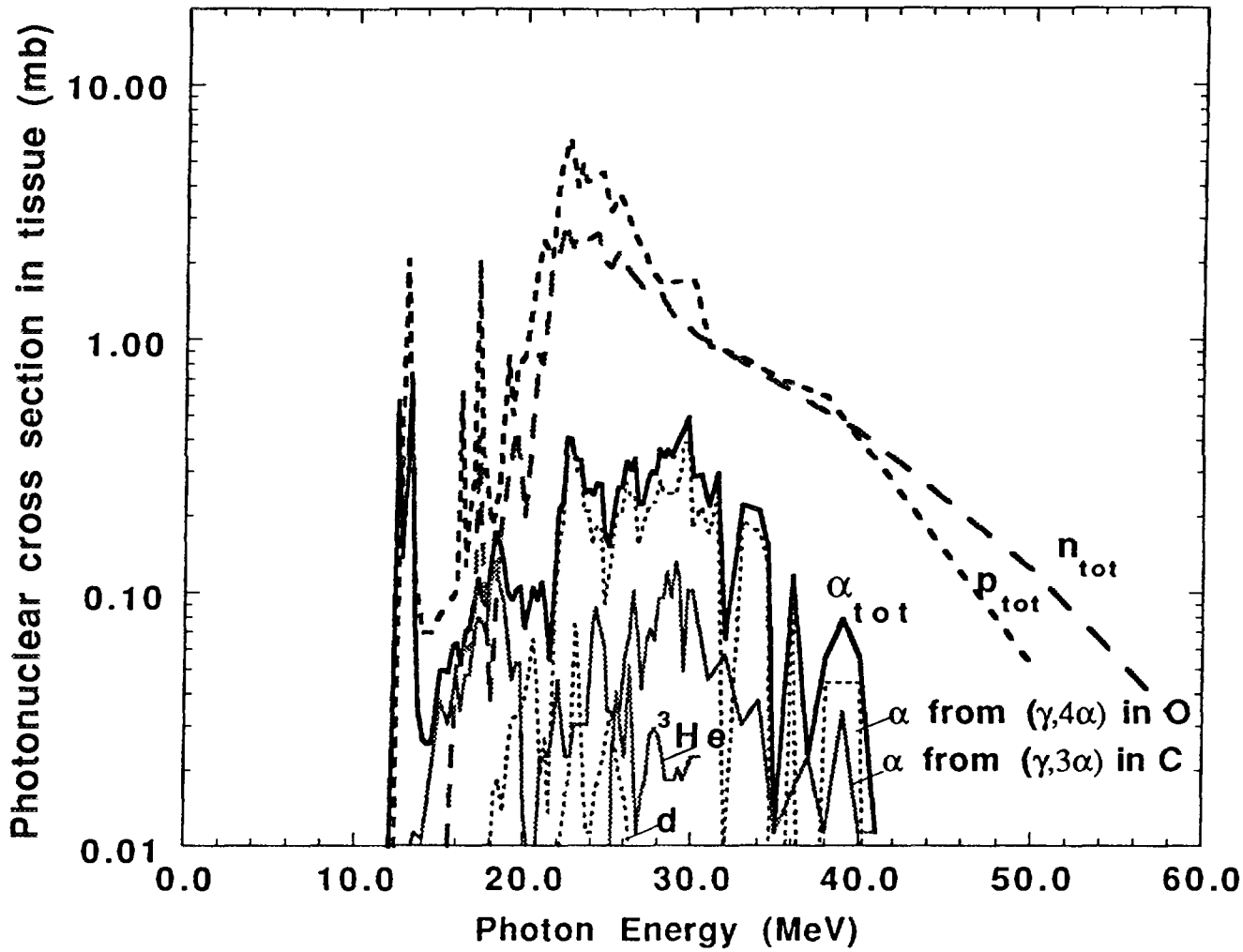

Fig. 12. Photonuclear cross section for neutron, proton, alpha, ^{3}He and deuteron production in tissue. The photonuclear cross section data for the constituent elements of soft tissue were taken from Fuller [38] and Vessière et al [40].

4.2. Calculation of the photon spectrum in tissue.

An evaluation of the bremsstrahlung spectrum from a Be-W target for a 50 MeV scanned electron beam has been performed using the Monte Carlo code ITS 3.0. The bremsstrahlung target consisted of 9 mm beryllium and 6 mm tungsten. The forward bremsstrahlung spectrum was calculated for an electron beam of perpendicular incidence on the target, and the final results were corrected for the oblique incidence (see sec. 3.1).

The transport of photons has been followed through the air between the target and a cylindrical phantom of tissue equivalent material of a thickness of 30 cm and radius of 50 cm. The surface of the phantom was placed at a distance of 100 cm from

the target. The photon energy spectra have been determined in phantom cells of 1 cm thickness for different distances from the isocenter and at different depths from the phantom surface.

The calculated photon energy spectrum at a depth of 5.5 cm on the central axis inside a tissue equivalent phantom is shown in Fig. 13.

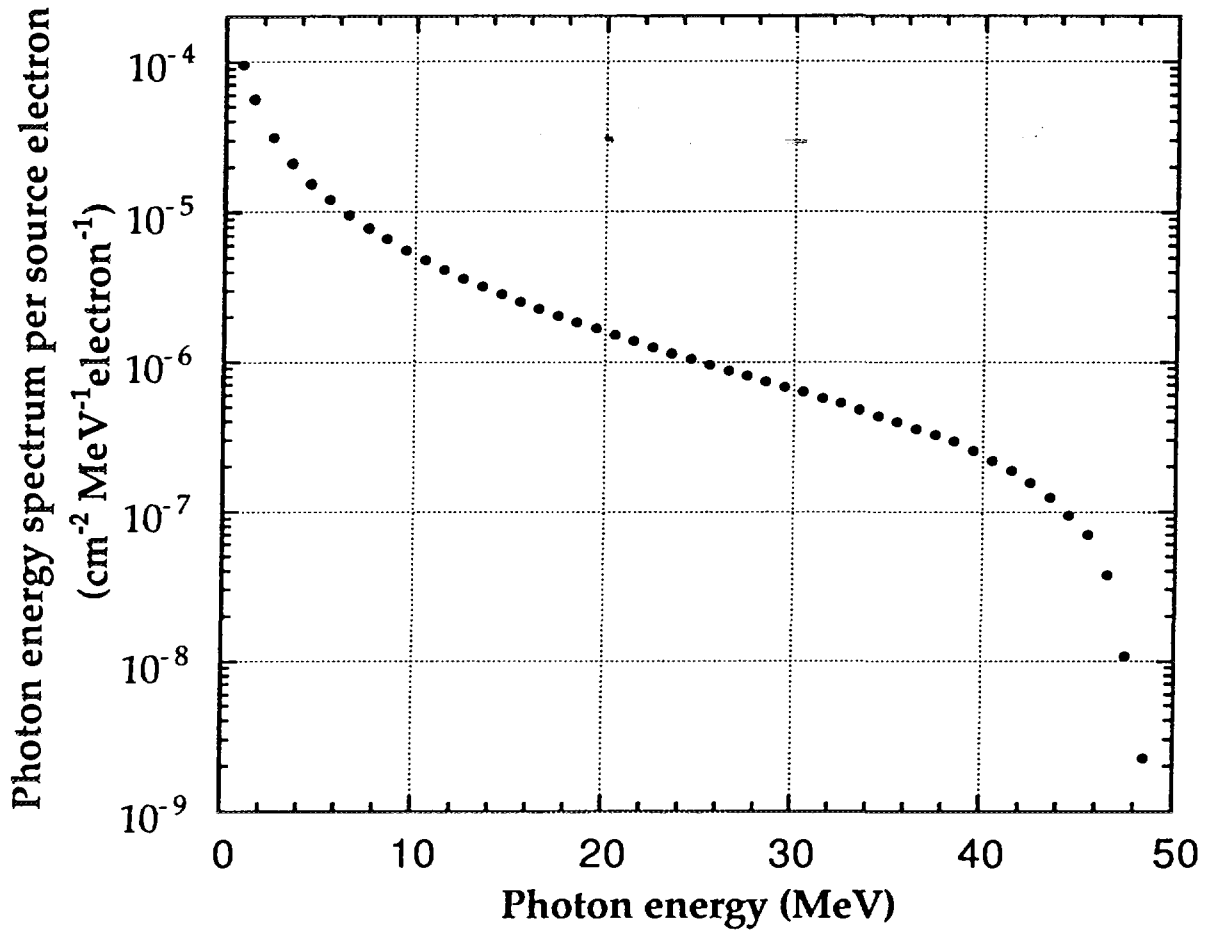

Fig. 13. Calculated photon energy spectrum per electron impinging on the target at the depth of 5.5 cm in tissue equivalent phantom.

To validate the photon energy spectrum evaluated by the Monte Carlo simulation, the photon absorbed dose delivered to the tissue at the depth 5.5 cm have been calculated and compared to the dose measured by a NACP ion chamber for the same operation mode of the racetrack. The ion chamber was placed inside a plexiglass phantom at the depth 5.5 cm from the phantom surface. During the measurements, the scanned electron beam on the target has been simultaneously monitored. Both calculated and measured photon absorbed doses have been normalized to electron impinging on the target. The difference between the calculated and measured results is about 27%, whereas the higher value of the

photon absorbed dose is given by the MC calculation. Similar finding has been discussed by other authors [41]. In the present investigations an error about 12% for the electron current and photon dose measurements, and an uncertainty about 15% in the calculated maximum photon dose can be assumed. The measured and calculated photon dose radial profiles for this depth agree within 10%.

4.3. Calculation of the neutron, proton and alpha particle spectra in tissue.

The photonuclear processes in the light elements like O, C, N are described by the direct process [37] in which the incident photon transfers its energy to a single particle which then is ejected from nucleus with an energy given by the difference between the photon energy and particle binding energy and possible excitation energy of the remaining nucleus.

The energy of the emitted photoparticle, E_p is given by:

$$E_p = (E_\gamma - E_t - E_e)\,(A - A_p)/A \qquad (4.1)$$

where:

E_γ is the photon energy

E_t is the threshold energy for the photonuclear reaction (particle binding energy)

E_e is the transition energy between excited-states of the residual nucleus

A is the mass number of the residual nucleus

A_p is the mass number of the emitted photoparticle

The factor $(A - A_p)/A$ is a correction for the recoil of the residual nucleus.

An analytical code has been used to calculate the neutron, proton and alpha particle spectra produced in the tissue by bremsstrahlung photons of the maximum energy of 50 MeV.

The photonuclear particle energy spectrum averaged over the unit volume of $1cm^3$, $n_{p,a}(E_p)$, for a single nuclide a and photonuclear particle p (neutron, protons alpha, ^{3}He particle etc.) of the energy E_p has been evaluated using:

$$n_{p,a}(E_p)\,dE_p = \sum_k \sum_j N_a\, c_k\, \sigma_{kj}(E_\gamma)\, \Phi_\gamma(E_\gamma)\, dE_\gamma \qquad (4.2)$$

where:

$\Phi_\gamma(E_\gamma)$ is the photon fluence energy spectrum

$\sigma_{kj}(E_\gamma)$ is the photoparticle production cross section for a given photonuclear reaction k ((γ, n), $(\gamma, 2n)$, (γ, pn), (γ, p), (γ, α), $(\gamma, 3\alpha)$, $(\gamma, 4\alpha)$ etc.) and for the excitation level j of the residual nucleus

c_k is a coefficient taking into account the number of particles produced in a

particular reaction

N_a is the number of nuclides per cm^3 (atomic density)

$n_{p,a}(E_p)$ is given in MeV^{-1} cm^{-3} per electron impinging on the target.

The angular distributions of the produced photoparticles from the light nuclei slightly peak at 90° [37]. However, to simplify the calculation an isotropic photoparticle production has been assumed in this evaluation.

The total photonuclear particle energy spectra in the tissue, $n_p(E_p)\,dE_p$, have been finally calculated as a sum of the single-nuclide spectra, $n_{p,a}(E_p)\,dE_p$ (eq. 4.2), weighted with the appropriate isotopic and atomic fractions.

The calculated energy spectra averaged over the volume of 1 cm^3 per electron impinging on the target for neutrons, protons, ^4He and ^3He particles produced in tissue equivalent phantom at the depth 5.5 cm on the central axis are shown in Fig. 14. The evaluated mean energies of neutrons, protons, alphas and ^3He particles produced in the tissue are 6.6, 7.9, 4.5 and 3.0 MeV respectively.

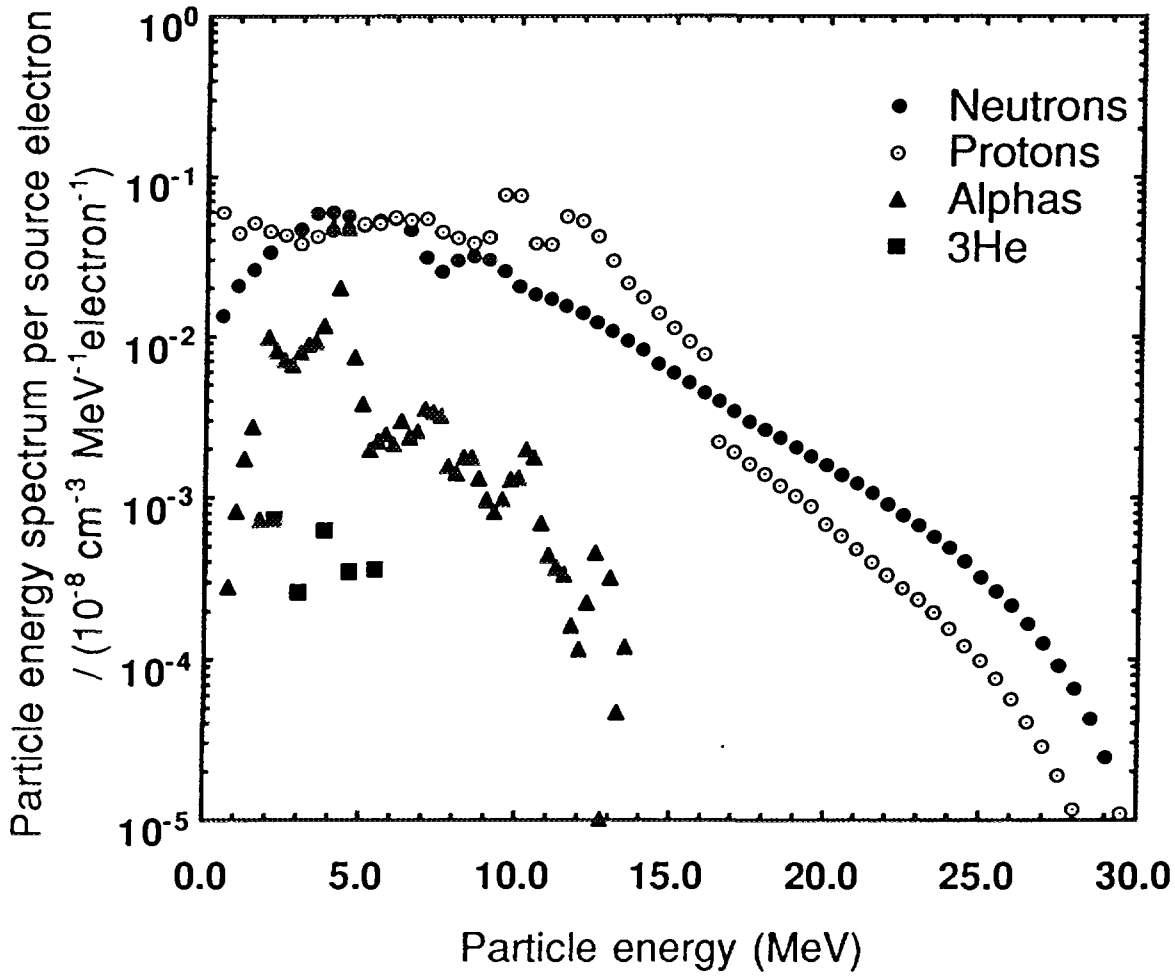

Fig. 14. Energy spectra of neutrons, protons, ^4He and ^3He particles averaged over the volume of 1 cm^3 per electron impinging on the target in tissue equivalent phantom at the depth 5.5 cm on the central axis.

4.4 Neutron transport and absorbed dose distribution determined with the MCNP4A code.

The photoneutron dose delivered to tissue either inside or outside the irradiated volume is affected by all neutrons produced by photons inside the target volume. Using the analytical code the photoneutron production inside the irradiation volume has been evaluated for a radiation field of 10x10 cm^2 at the phantom surface . The calculations were performed for twenty cells of the thickness 1 cm, placed from the phantom surface to the depth of 20 cm. The photoneutron production in the respective cells was averaged over the volume of the cells. The neutron energy distributions in the cells have been used as input neutron source to the MCNP4A Monte Carlo code. The photoneutron transport has been simulated inside a tissue equivalent phantom of the size 40x40x30 cm^3. Fig. 15 shows a cross sectional view of the phantom with the cells as coded in the MCNP4A code. The neutron sources due to photoneutron reactions in the irradiated volume were defined in the cells numbered from 101 to 120. The absorbed doses of neutrons and gamma radiation due to neutron induced photons in the tissue were determined for positions inside and outside the irradiated volume. The calculations were performed for the cells of the volume of 1 cm^3 numbered from 201 to 223.

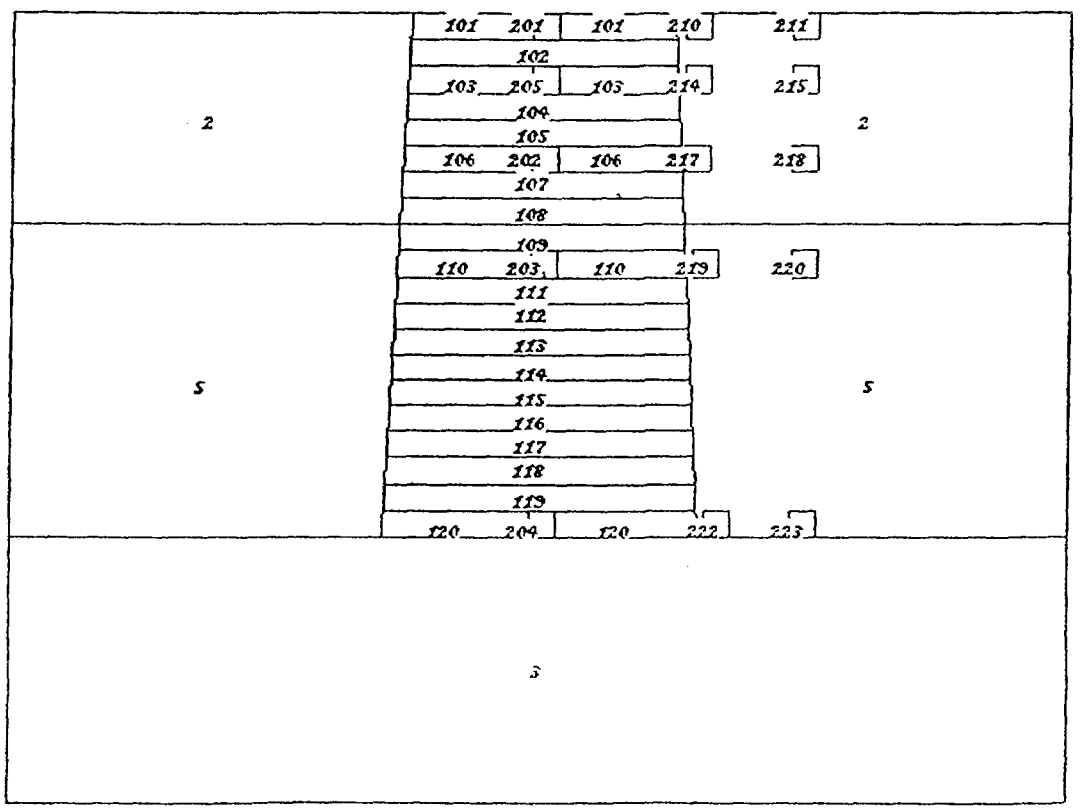

Fig. 15. A cross section view of the tissue equivalent phantom with the cells as coded in the MCNP4A code.

The absorbed dose per maximum photon dose due to neutrons and gamma radiation from neutron induced gammas in the tissue are shown in the Table V. In this calculation only promt gamma i.e. that produced at the time t equal to zero were taken into account. The maximum photon dose in tissue per electron impinging on the target was calculated using the photon energy spectrum from the simulation by ITS 3.0.

The absorbed photoneutron dose to the tissue on the central axis is about 0.014% of the maximum photon dose over the depth range 2.5 - 9.5 cm. At the depth of 19.5 cm the photoneutron dose is ten times lower than the dose at the depth of 5.5 cm. Ouside the irradiated volume at the distance 10 cm from the isocenter the photoneutron absorbed dose is from 7 to 10 times lower than the dose on the central axis. The gamma absorbed dose due to neutron induced gammas determined on the central axis is about 20 times lower than photoneutron absorbed dose.

4.5 Determination of the absorbed dose due to protons, alpha and ^{3}He particles.

Since the mean range of the produced photoparticles, protons, alphas and ^{3}He particles in tissue is less than 1mm as calculated using the Monte Carlo Ion Transport code TRIM95 [42, 43], the photonuclear absorbed dose was evaluated with the assumption of charged particle equilibrium (CPE).

The photonuclear absorbed dose, D_p, for protons, alphas and ^{3}He particles have been calculated using the relation:

$$D_p = \sum_{Ep} n_p(E_p)\, E_p\, dE_p \qquad (4.3)$$

where:

$n_p(E_p)$ is the number of particles p with energy E_p calculated per unit mass using the equation 4.2.

The calculated absorbed dose in tissue at the depth 5.5 cm due to protons, alphas and ^{3}He particles is shown in Table VI.

The absorbed dose in tissue due to protons, ^{4}He and ^{3}He particles are about 0.09, 0.005 and 0.0001 % of the maximum photon dose.

Table V.

The photoneutron absorbed dose and gamma absorbed dose due to neutron induced gammas in tissue, per maximum photon dose calculated using the MCNP4A code.

Cell number and position inside the phantom	Photoneutron absorbed dose mGy/Gy	Gamma absorbed dose mGy/Gy
201 (0.5, 0.0)	0.101	0.003
205 (2.5, 0.0)	0.136	0.003
202 (5.5, 0.0)	0.145	0.006
203 (9.5, 0.0)	0.142	0.004
204 (19.5, 0.0)	0.071	0.004
210 (0.5, 6.0)	0.041	0.001
214 (2.5, 6.1)	0.055	0.003
217 (5.5, 6.1)	0.067	0.004
219 (9.5, 6.2)	0.064	0.005
222 (19.5, 6.7)	0.030	0.004
211 (0.5, 10.0)	0.012	0.003
215 (2.5, 10.0)	0.016	0.001
218 (5.5, 10.0)	0.021	0.002
220 (9.5, 10.0)	0.022	0.002
223 (19.5, 10.0)	0.014	0.002

Cell position (a, b) in cm inside the tissue equivalent phantom: a - position along the central axis, b - distance from the central axis in the plane parallel to the isocenter plane, position (0.0, 0.0) at 1 m SID.

cells 201 - 205 inside the irradiated volume, on the central axis

cells 210, 214, 217, 219, 222 outside the irradiated volume, near the edge

cells 211, 215, 218, 220, 223 outside the irradiated volume, 10 cm from the isocentre

4.6 Discussion.

The total photonuclear absorbed dose in tissue consists of the contributions due to photonuclear particles produced in the tissue and due to photoneutrons produced in the accelerator and transported to the tissue. The accelerator produced neutrons have approximately the isotropic distribution around the patient body.
Table VI shows the results of the evaluated photonuclear absorbed dose per maximum photon dose in the soft tissue at the depth of 5.5 cm inside the irradiated volume.
The contribution from neutrons produced in the treatment head and scattered from the inside structure of the treatment room, and transported to this depth has been evaluated from the measured photoneutron absorbed dose at the phantom surface (see sec.2.4 and chap. 5).
The calculated photonuclear dose due to protons, ^{4}He and ^{3}He particles is about 69, 3.9 and 0.1 % of the total photonuclear absorbed dose, respectively whereas the contribution due to all photoneutrons in the tissue is about 27 %.

The total photonuclear absorbed dose to patient is about 0.1% of the maximum photon dose.

Table VI.

The photonuclear absorbed dose per maximum photon dose to tissue in % at the depth 5.5 cm inside the irradiated volume. The 50 MeV electrons on the 9Be6W target, scanned mode, 10x10 cm^2 at 1m SID

Source	Photoneutrons from accelerator (measured)	Neutrons produced in tissue due to (γ,xn) reactions	Protons produced in tissue due to (γ,xp) reactions	Alphas produced in tissue due to (γ,xα) reactions	3He particles produced in tissue due to (γ,^{3}He) reactions	Total photonuclear absorbed dose to tissue
Dose delivered to tissue	0.02	0.015	0.09	0.005	0.00012	0.13

The statistical error of the Monte Carlo simulation of bremsstrahlung spectrum by ITS 3.0 is about 2% (1 σ) for the calculation with 10 000 histories. The statistical error of the simulation of neutron absorbed dose in tissue using MCNP4A is about 2% (1 σ) for the 1 000 000 histories. The systematic error due to uncertainty of the

photoneutron cross section data for oxygen, carbon and nitrogen is from 5 to 20% [38] depending of the photon energy and nuclide. The systematic error of the photoproton cross sections in tissue is about 15% [38]. The cross section data for photoalpha production bare a systematic error about 20% for photons up to 30 MeV and about 40% for photons up to 50 MeV for oxygen and carbon [38]. The error due to the calculation of maximum photon dose is about 10%. In addition the uncertainty in the description of the geometry for the scanned photon beam transport contributes to the systematic error. The total calculation error is about 25% (1σ).

One should also remember that the bremsstrahlung spectrum in tissue was evaluated for photon transport for a simple geometry target - air - tissue equivalent phantom, instead for the whole true treatment head geometry. In the future more careful calculation of photon transport in the treatment head and tissue equivalent phantom using MCNP4B is planned.

The photonuclear absorbed dose estimated by the procedure presented above, can be compared to the photonuclear dose of 2.0 % determined by the microdosimetric measurements [5]. The microdosimetric measurements have been performed for the similar bremsstrahlung beam of 50 MV but of the different scanning pattern of about 15 cm in diameter at 1m SID. In the microdosimetric measurements the tissue equivalent detector with the A-150 TE plastic and the methane based TE gas was used. The differences in the elemental composition of the used tissue equivalent materials in both methods and different geometry of the scanned beam would hardly explain a large discrepancy (about 15 times) between calculation and measurements. Thus, a new microdosimetric measurement and an improved calculation of the photonuclear dose delivered to the material of the microdosimetric detector with a careful evaluation of the photon energy spectrum in tissue are necessary.

5. Radiation effects to the patient due to radiation therapy with high energy photons.

The absorbed dose due to photoneutrons from the treatment head per unit photon dose at dose maximum was 0.044% at 1m SID at the centre of the 10x10 cm^2 field for 50 MV photons from the racetrack microtron in the scanned mode. This absorbed dose was determined in the soft tissue at the depth about 1cm from the skin surface using the fluence-to-absorbed dose conversion factor from the NCRP Report No. 79 [1], which refers to the data from ICRP Publication 21 [30]. Additionally, a photoneutron absorbed dose of about 0.01% was produced inside the body at the depth 1.0 cm. Since the photoneutron spectrum in the patient plane due to accelerator produced neutrons has a mean energy of about 1 MeV a radiation weighting factor of about 20 [44] can be used to estimate the equivalent dose for radiation protection purposes. The photoneutron absorbed dose in the patient plane decreases by factors of about 0.9, 0.74 and 0.62 at the 10, 30, 50 cm distances from the isocentre respectively (see Fig. 10). This means that the dose equivalent to the surface tissues at the distances 0, 10, 30, 50 cm from the isocentre is about 1.08, 0.79, 0.65 and 0.55 %, respectively. For a whole treatment course with a photon dose of 60 Gy the photoneutron equivalent dose at these distances is about 650, 470, 390 and 330 mSv. Similar values of the photoneutron dose equivalent have been estimated for 18 - 21 MV treatment units. The dose equivalent of neutrons at the isocentre is about 1.0% of the maximum photon dose, whereas at a distance 50 cm from the isocentre it decreases to value of about 0.6%. Outside the primary photon beam up to 30 cm from the isocenter the absorbed dose to the patient skin is mainly due to secondary electrons and scattered primary photons. For the 15 - 21 MV photon beams this dose is from 10 to 50 % of the primary photon dose depending on the gantry design and the radiation field size [45]. However, at the distances larger than 30 cm from the isocenter the dose due to secondary electrons and scattered primary photons is negligible whereas photoneutrons contribute to the dose equivalent to the healthy tissues on the level of 0.3 - 0.6 % of the maximum photon dose.

For tissues, situated inside the patient body the photoneutron absorbed dose due to accelerator produced neutrons can be estimated using the neutron attenuation with depth below the body surface [31, 46]. For example at the distance 5.5 cm from the surface of the water phantom the neutron absorbed dose is about 0.42 of the surface dose for the 50 MV photon beam [46]. For our case the neutron absorbed dose is about 0.019% at the central axis at this depth. The neutron absorbed dose due to photoneutron reactions in the soft tissue is 0.015% at this depth. The total

photoneutron dose in the tissue at the depth 5.5 cm is about 0.034%.
It can be assumed that the attenuated neutron spectrum at the depth 5.5 cm in the soft tissue has a radiation weighting factor of about 10. In this case the photoneutron dose equivalents in soft tissue at distances of 0, 10, 30 and 50 cm from the central axis are about 200, 100, 85 and 70 mSv respectively for a photon dose of 60 Gy.
The estimated photoneutron dose equivalent to the tissues inside and outside the treated volume do not exceed the recommended values [47]. However, there is a potential risk that sensitive tissues (lens of the eye or gonads), outside the treatment volume, can receive a dose of about 300 - 500 mSv per the treatment course of 60 Gy with a slightly increase for secondary malignancies.

6. Conclusions.

Photonuclear reactions around the MM50 Racetrack microtron at the Karolinska Hospital contribute to the total radiation dose delivered to the patient both inside and outside the treated volume and the level is dependent both on the mode of operation and the acceleration potential.

The measured photoneutron absorbed dose to the patient due to accelerator produced neutrons varies from about 0.044 to 0.027% of the photon dose at dose maximum over the distance range from 0 to 0.5 m from the isocenter for a scanned beam of 50 MV photons and a radiation field size 10 x 10 cm^2 at 1m SID. For this operation mode the photoneutron absorbed dose in the patient plane decreases to 0.013% at 1 m distance from the isocenter.

The photoneutron absorbed dose at isocenter at 1m SID and the radiation field 10 x 10 cm^2 is about 4.5 times larger for the scanned 50 MV photons operated with the maximum scanning pattern than for the photon beam operating in the stationary mode. In the scanned mode a larger volume of shielding materials is penetrated by high energy photons and for a given photon dose at isocenter many more photons are emitted from the target when compare to the stationary mode. In consequence a higher photoneutron production is observed for the scanned mode.

This indicates a large influence of the individual scanning pattern for the treated volume. The clinical requirement is to decrease the patient exposure to unnecessary neutrons and thus to minimize the scanned area.

The fast neutron fluence measurements both inside and outside the treated volume for scanned bremstrahlung beams in the range 10 - 50 MV showed the increasing photoneutron production with the acceleration energy up to 30 MV. Between 30 and 50 MV almost constant neutron yield is observed in agreement with the other observations [7].

At the depth 5.5 cm on the central axis the contribution of the photoneutron absorbed dose to the total therapy dose is about 0.02 and 0.15% of the photon maximum dose due to the accelerator produced neutrons and photoneutrons produced by photonuclear reactions in tissue, respectively. The latter contribution has been evaluated using computer simulation. The bremsstrahlung production in the target and photon beam transport through the air and tissue equivalent phantom have been performed using the Monte Carlo code ITS 3.0. Annalytical calculation was used to evaluate the photoneutron production, whereas photoneutron transport and energy deposition to the tissue have been evaluated using the Monte Carlo code MCNP4A. Photonuclear production of other photonuclear particles like protons, ^4He, ^3He and deuterons produced inside the treated volume have been evaluated by convolution of the photon energy spectrum

in the tissue with the photonuclear cross section of the tissue constituents. The photonuclear dose due to protons, ^4He, ^3He and deuterons produced at the depth 5.5 cm by 50 MV bremsstrahlung scanned beam contribute to the total photonuclear dose by 73%, with the largest contributions of 69% due to photoprotons. The total photonuclear absorbed dose in tissue delivered to the treated volume is about 0.1% of the maximum photon dose.

In this calculations several simplifications, mainly concerning the geometry setup for the particle transport, have been applied. That was necessary to do since both codes ITS 3.0 and MCNP4A use different approach to describe the geometry for the problem. In ITS 3.0 the combinatorial method with the problem input zones built up of primitive bodies is applied, whereas in MCNP4A a more general geometry of geometric cells bounded by first- and second -degree surfaces is used. In addition, due to bugs in the ITS 3.0 code for the oblique beams the bremsstrahlung production and photon transport were calculated for a pencil beam impinging perpendicularly on the target and corrected later for the scanned beam mode. Because of this, photon transport was evaluated for a simplified geometry target - air - tissue equivalent phantom, instead for the whole true treatment head geometry. It is probable that this approach may not give the correct photon energy distribution in the high energy region which directly influences on the photonuclear production in the tissue.

Part of this project was related to computer simulation of neutron sources, neutron transport and neutron fluence inside the treatment room of a MM50 racetrack microtron. The ITS 3.0 code was used to evaluate the bremsstrahlung spectrum from a 9Be6W target and to follow photon transport in the treatment head. The photoneutron sources in the treatment head were calculated analytically and neutron transport inside the treatment room and calculation of the fast neutron fluence were simulated using MCNP4A. Because of the reasons discussed above these calculations were also simplified and resulted in the very approximative determination of the photoneutron sources in the cells of the treatment head. The calculated fast neutron fluences in the patient plane are in the large discrepancy from the measured data by factor from 1.5 to 3.5 depending on the distance from the isocenter.

The evaluation of photoneutron radiation in the treatment room of the MM50 Racetrack microtron as well as the calculation of photonuclear absorbed dose delivered to tissue for the photon therapy beam in the scanned mode can be improved by using the MCNP4B or the FLUKA 93/94 codes.

In the version MCNP4B a continous-energy electron transport, and a thick target

bremsstrahlung production and transport implemented from the ITS 3.0 code is added to neutron transport. It means that in MCNP4B code the geometry of the treatment head and treatment room is defined in the same way for electron, photon and neutron transport that makes the evaluation of photonuclear particle sources more correct and more simple. In the MCNP4B code the problems of describing the oblique geometry are eliminated.
On the other hand in FLUKA 93/94 transport of electrons, photons and photonuclear particles is followed in one package, that makes this code an attractive tool to evaluate photon and neutron radiation around high energy medical electron accelerators.

The use of these powerful Monte Carlo codes to simulate the photoneutron spectra in the patient as well as inside and outside the treatment room is of high importance for radiation protection purposes. An accurate knowledge about the photoneutron spectrum is necessary in order to apply the correct radiation quality factor Q(L). The last recommendations on radiological protections presented in ICRP Publication 60 [44] introduced significant changes with respect to neutron radiation quality weighting. The new Q(L) relation recommended in ICRP Publication 60 results in an increase of the quality factor for neutrons of up to 50% depending on neutron energy. Therefore, a special care should be given to the photoneutron equivalent dose in the organs at risk by calculation of the absorbed dose both due to accelerator produced neutrons and neutrons produced in tissue and scattered outside the treatment volume using the new radiation weighting factors, wR, [44]. Especially the accurate evaluation of the photoneutron spectrum in the patient due to photoneutrons produced in the treatment head and scattered from the inside structure of the treatment room is of importance since the whole body of the patient is affected by this radiation. It is well known that high LET photonuclear particles like neutrons are associated with an increased risk of inducing cancer in healthy tissues.

The estimated neutron equivalent dose due to accelerator produced neutrons by photon beams from MM50 Racetrack microtron delivered to the tissues inside and outside the treatment volume do not exceed the recommended values [47]. However there is a potential risk that the sensitive tissues like the lens of the eye or the gonads, outside the treatment volume, can receive the dose of about 300 - 500 mSv per the treatment course of 60 Gy_{γ}.

Also, the energy distribution of neutrons transported outside the treatment room is very important in order to evaluate the radiation risk for personnel in the therapy

and accelerator control rooms. Measurements of photoneutron fluences in these zones showed a low level. However, the evaluation of the photoneutron absorbed dose delivered to personnel is impossible without the knowledge about neutron energy distribution in these rooms, which are specific for every accelerator.
The application of the MCNP4B and FLUKA-93/94 codes to simulate the radiation field around the medical electron accelerator will improve the evaluation of the photon and neutron radiation to the working hospital personnel and allows for more careful evaluation of the equivalent dose to patient.

Acknowledgements.

Peder Näfstadius (KS) helped to run MM50 racetrack microtron at the Karolinska Hospital. Pedro Andreo (KI/SU) performed the calculation of the bremsstrahlung spectrum using the ITS 3.0 code. Waclaw Gudowski (KTH) and Jesper Kierkegaard (KTH) helped with the test calculations using the MCNP4A code.
The stimulating discussions with Anders Brahme, Lennart Lindborg, Roger Svensson, Aris Tilikidis and Bengt Lind are gratefully acknowledged.

The project was supported by the Swedish Radiation Protection Institute.

References.

1. NCRP, Neutron Contamination from Medical Electron Accelerators, Report No. 79, 1984.
2. Nordell, B., Nucl. Instr. Meth., 224, 547, 1984.
3. McCall, R.C., private communication, 1985.
4. LaRiviere, P. D., Neutron energies in medical electron accelerator rooms, Med. Phys. 12 (6), 769,1985.
5. Tilikidis A., Lind B., Näfstadius P. and Brahme A. ,An estimation of the relative biological effectiveness of 50 MV scanned bremsstrahlung beams by microdosimetric techniques, Phys. Med. Biol. 41, pp. 55 - 69, 1996.
6. Zackrisson B. and Karlsson M., Relative biological effectiveness of 50-MV x-rays on jejunal crypt survival in vivo, Rad. Res. , 113 pp. 112-114, 1992.
7. NBS Special Publication 554, ed. Heaton II, H.T. and Jacobs, R., Procc. of a Conference on Neutrons from Electron Medical Accelerators, 1979.
8. Nath, R., Epp, E.R., Laughlin, J.S., Swanson, W.P. and Bond, V.P., Med. Phys. 11 (3), 231,1984.
9. Gudowska I., Internal Report. Dept. of Radiation Physics, The Karolinska institute, Stockholm, RI 1985-02 ,1985.
10. Uwamino, Y., Nakamura, T., Ohkubo and Hara, A., Med. Phys. 13 (3), 374,1986.
11. Gudowska, I., Rad. Prot. Dosim. Vol. 23 No. 1/4, 345, 1988.
12. McGinley, P.H. and Landry, J.C., Phys. Med. Biol. 34, No 6, pp. 777-783, 1989.
13. Tosi, G. Torresin, A., Agosteo, S., Foglio Para, A., Sangiust, V., Zeni, L. and Silari, M., Med. Phys. 18 (1), 54,1991.
14. Agosteo S., Foglio Para A., Gerardi F., Silari M., Torresin A. and Tosi G., Nucl. Instrum. Methods B 72, pp. 84-90, 1992.
15. Manfredotti C., Nastasi U., Ornato O. and Zaninni A., Rad. Prot. Dosim. Vol. 44 No. 1/4, pp.457-462, 1992.
16. Agosteo S., Foglio Para A., Gerardi F., Silari M., Torresin A. and Tosi G., Phys. Med.Biol. 38 pp.1509-1528, 1993.
17. McGinley, P.H., Radiation Protection Management, Vol. 10, No 5, p. 59, 1993.
18. McGinley, P.H., Ghavidel S. and Landry J., Radiation Protection Management, Vol. 10, No 1, pp. 45-50, 1993.
19. Nath, R., Meigoni, A.S., King, C.R., Smolen, S. and d'Errico, F., Med. Phys. 20 (3), 781,1993.
20. Agosteo, S. and Foglio Para, A., Nucl. Instrum. Methods B 93, 362, 1994.
21. McGinley, P.H. et al , Phys. Med. Biol., (40) 1995, p.1467.

22. Kleck, H., Elsalim, M.M., Teachout, A.J., Englert, A.J., Liu, J.C., Nelson, W.R., Kase, K. and Mao, X.S., Eight Symposium on Neutron Dosimetry, Paris, 13-17 November, 1995.
23. Crossman, J.S.P. and Watt, D.E., Eight Symposium on Neutron Dosimetry, Paris, 13-17 November, 1995.
24. Brahme, A., Proc. Workshop on Principal Aspects of High Energy Electron Accelerators in Radiation Therapy, 3-8 Dec. 1982, ed. K. R. Das, p. 263.
25. Gudowska, I., Internal Report. Dept. of Radiation Physics, The Karolinska institute, Stockholm, RI 1984-04 ,1984.
26. McCall, R.C., SLAC-PUB-2739, May, 1981
27. McGinley, P.H., Wood, M., Mills, M. and Rodrigues, R., Med. Phys. 3 (6), 397,1976.
28. Andersson, T.L. Aktiebolaget Atomenergi Report, AE-229, 1966.
29. Svensson, R. and Brahme, A., Phys. Med. Biol., (41), 1996, pp.1353-1379.
30. ICRP Publication 21, Recommendations of the International Commision on Radiological Protection, Data for Protection against Ionizing Radiation from External Sources, 1971.
31. McCall, R.C. and Swanson, W.P., NBS Special Publication 554, p.75, 1979.
32. Halbleib J.A., Kensek R.P., Mehlhorn T.A., Valdez G.D., Seltzer S.M. and Berger M.J., ITS Version 3.0: The Integrated TIGER Series of Coupled Electron/Photon Monte Carlo Transport Codes, SAND91-1634, UC - 405, 1992.
33. Blatt, J. and Weisskopf, V.F., "Theoretical Nuclear Physics", John Wiley & Sons, Inc., New York, 1952.
34. Dietrich S. S. and Berman B. L., Atlas of photoneutron cross sections obtained with monoenergetic photons, Atomic data and nuclear data tables, 38, pp. 199-338, 1988.
35. Briesmeister J. and Hendricks J. MCNP4 Newsletter X-6:JFB-91-177 (1991) Los Alamos, NM: Los Alamos National Laboratory.
36. Fassó, A., Ferrari, A., Sala, P., Ranft, J., Asrnio, P., Moehring, J.-H., Stevenson, and Zazula, J.M., "FLUKA-93/94", manual, CERN 1995.
37. Hayward, E., Photonuclear reactions, NBS Monograph 118, 1970.
38. Fuller E.G., Photonuclear reaction cross sections for ^{12}C, ^{14}N and ^{16}O, Physics Reports 127, No. 3, pp. 185 - 231, 1985.
39 ICRU Report 44, 1989.
40. Veyssière A., Beil H., Bergere R. et al, A study of the photoneutron contribution to the giant dipole resonance of s-d shell nuclei, Nucl. Phys. A227, p.513, 1974.
41. Sätherberg A., Andreo P. and Karlsson M., Med. Phys. 23 (4), 495,1996.
42. Biersack, J.P. and Haggmark, L., Nucl. Instr. Meth., 174, 257, 1980.

43. TRIM - 95, The transport of ions in matter, Instruction Manual, J. F. Ziegler, IBM-Research, 1995.
44. ICRP Publication 60, 1990 Recommendations of the International Commision on Radiological Protection, 1991.
45. Nilsson B, Thesis, Department of Radiation Physics, KI/SU, Stockholm, Sweden, (1985).
46. Brahme A., Montelius A., Nordell B., Reuthal M. and Svensson H., Investigation of the possibility of using photoneutron beams for radiation therapy, Phys. Med. Biol. Vol. 25 (6), 1980, pp.1111-1120.
47. ICRP Publication 33, 1981.